The Astrophysical Journal, 994:176 (21pp), 2025 December 1 https://doi.org/10.3847/1538-4357/ae0e21
© 2025. The Author(s). Published by the American Astronomical Society.
OPEN ACCESS

The Stellar Content of NGC 3603 Revisited: Is the IMF Top Heavy?*

Philip Massey[1,2], Nidia I. Morrell[3], Kathryn F. Neugent[1], Monica Herzog[1,2,5], Maria R. Drout[4], and Caitlin O'Brien[1,2,6]
[1] Lowell Observatory, 1400 W. Mars Hill Road, Flagstaff, AZ 86001, USA
[2] Department of Astronomy and Planetary Science, Northern Arizona University, Flagstaff, AZ 86011-6010, USA
[3] Las Campanas Observatory, Carnegie Observatories, Casilla 601, La Serena, Chile
[4] David A. Dunlap Department of Astronomy and Astrophysics, University of Toronto, 50 St George Street, Toronto, ON M5S 3H4, Canada
Received 2025 August 27; revised 2025 September 26; accepted 2025 September 29; published 2025 November 25

Abstract

Studies of the resolved stellar populations of young massive clusters have shown that the slope of the initial mass function (IMF) appears to be the same everywhere, with no dependence on stellar density or metallicity. At the same time, studies of integrated properties of galaxies usually conclude that the IMF does vary and must be top-heavy in starburst regions. In order to investigate this, we have carried out a long-term project to characterize the massive-star content of NGC 3603, the nearest giant H II region, known to have a rich population of massive stars. We used both ground-based and Hubble Space Telescope (HST) imaging to obtain photometry, and we employed Gaia to establish membership. We obtained spectra of 128 stars using the Magellan 6.5 m telescope and HST, and we combine these data to produce a reddening map. After analyzing the data in the same way as we have for 25 other star-forming regions in the Milky Way and the Magellanic Clouds, we find that the IMF slope of NGC 3603 is quite normal compared to other clusters, with $\Gamma = -0.9 \pm 0.1$. If anything, there are fewer very high mass ($>65 M_{\odot}$) stars than one would expect by extrapolation from lower masses. This slope is also indistinguishable from what several studies have shown for R136 in the LMC, an even richer region. We speculate that the depreciation of the highest-mass bins in NGC 3603, but not in R136, may indicate that it is harder to form extremely massive stars at the higher metallicity of the Milky Way compared to that of the LMC.

Unified Astronomy Thesaurus concepts: Initial mass function (796); Massive stars (732); Stellar evolution (1599)

Materials only available in the online version of record: machine-readable tables

1. Introduction

One of the outstanding puzzles of star formation concerns the apparent universality of the initial mass function (IMF). E. E. Salpeter (1955) showed that when stars are formed there are a decreasing number of stars with increasing mass and that this was well represented by a power law. If we describe the IMF as $\xi(m) \propto m^{\Gamma-1}$, then for stars more massive than $0.5 M_{\odot}$, $\Gamma = -1.3 \pm 0.5$ (P. Kroupa 2007). This Γ is referred to as the "slope of the IMF," and the ± 0.5 on its value is based on the normal variation seen from one OB association or cluster to another and does not seem to be correlated with metallicity or star density (P. Massey 1998, 2011; B. G. Elmegreen 2005); it may simply represent the stochastical nature of sampling of a probability function (P. Kroupa 2001, 2002).[7]

This universality of the IMF is surprising. For instance, one would naively expect that the reduced effect of radiation pressure during the accretion phase of star formation would favor the formation of higher-mass stars in lower-metallicity environments such as the SMC compared to that of the Milky Way. It must be that other factors dominate. The persistence of the IMF despite such stellar feedback is one of the great challenges in understanding star formation (see, e.g., B. G. Elmegreen 2011). In fact, to some extent, star formation theorists are still struggling to understand why the stellar IMF is a power law at all; modern explanations focus on cloud fragmentation driven by supersonic turbulence and self-gravity, clump coalescence, and protostellar accretion (see, e.g., M. Shadmehri & B. G. Elmegreen 2011, and references therein), but the relative importance of these processes is still uncertain.

However, an exception to this universality *may* exist where the star formation rates (SFRs) are extremely high. Some experts assert that the IMF is flatter ("top-heavy") in such starburst regions. This evidence comes primarily from unresolved stellar populations and traces at least as far back as J. P. Huchra (1977), who found that blue galaxies (and hence ones with lots of active star formation) must have IMF slopes flatter than Salpeter in order to match their broadband colors and Hβ emission. The notion was further ingrained in our collective consciousness as a result of the G. H. Rieke et al. (1980) study of the starburst galaxy M82. (It was this study that coined the phrase "top-heavy" to indicate the relative absence of low- and intermediate-mass stars.) However, subsequent work by the same group showed that it was not true (G. H. Rieke et al. 1993). The notion of a top-heavy IMF in starburst galaxies was further promoted by J. Scalo

* This paper includes data gathered with the 6.5 m Magellan Telescopes located at Las Campanas Observatory, Chile. It also uses observations made with the NASA/ESA Hubble Space Telescope (HST), obtained at the Space Telescope Science Institute, which is operated by the Association of Universities for Research in Astronomy, Inc., under NASA contract NAS 5-26555. These observations were made under proposals GO-10602 (PI: Maiz Apellaniz) and GO-11626 (PI: Massey).
[5] NSF REU student 2012.
[6] NSF REU student 2021.
[7] The canonical "Salpeter" value is −1.35, although H. Zinnecker (2011) has pointed out that if E. E. Salpeter (1955) had used the modern value for the age of the Milky Way's disk, he would have derived $\Gamma = -1.05$ (P. Kroupa & T. Jerabkova 2019). We also note that Salpeter's sample did not contain any O stars, although it is used as the standard for massive stars.

Original content from this work may be used under the terms of the Creative Commons Attribution 4.0 licence. Any further distribution of this work must maintain attribution to the author(s) and the title of the work, journal citation and DOI.

(1990; despite the reversal on M82), although he notes that the results could be just as well explained if the upper mass limit were higher than $80M_{\odot}$–$100M_{\odot}$. Similarly, G. R. Meurer et al. (2009) invoke a top-heavy IMF to explain the correlation of flux ratio of Hα to the far-UV to global properties in a sample of H I–selected galaxies, although systematic variations in the upper mass limit would also match their models. Not all studies of the integrated properties of starburst regions agree. For instance, C. Leitherer (2011) finds no evidence of environmental effects on the IMF in starburst regions and distant star-forming galaxies using population synthesis models based on UV spectral lines. A recent study of the transient frequency in the lensed Spock arc by S. K. Li et al. (2025) shows that the data are consistent with a Salpeter IMF, and not with a top-heavy IMF, contrary to the usual assumptions about star formation in the early Universe.

Despite the results of studies of resolved stellar populations, the idea that starburst regions have top-heavy IMFs has continued to gain traction, with the two nearest giant H II regions, NGC 3603 in the Milky Way and R136 in the LMC, often cited as examples where this is the case. In part this may be driven by the belief that from a theoretical perspective such regions "should" have a flatter IMF. Some may also take the canonical Salpeter $\Gamma = -1.35$ value as an absolute standard, not fully recognizing that slight variations are seen, as described above. Finally, there is also the fact that researchers will derive slightly different temperatures and luminosities for the same stars. In R136, P. Massey & D. A. Hunter (1998) find $\Gamma = -1.3 \pm 0.2$. For a more extended region in 30 Dor, F. R. N. Schneider et al. (2018) derive $\Gamma = -0.90^{+0.26}_{-0.37}$, again, well within the normal variations seen for the IMF slope in young massive clusters, yet describe their result as showing an "excess of massive stars." J. M. Bestenlehner et al. (2020) conducted a similar study in R136 and, using more advanced modeling techniques, derive $\Gamma = -1.0 \pm 0.3$, which also agrees well with previous values.

The case for NGC 3603 is more confused. Y. Harayama et al. (2008) found an IMF slope of $\Gamma = -0.74^{+0.62}_{-0.47}$, which they describe as top-heavy. While the value is flatter than a Salpeter $\Gamma = -1.35$, it is still well within the range we see in less extreme regions, such as NGC 6611, for which L. A. Hillenbrand et al. (1993) find $\Gamma = -0.7 \pm 0.2$. The Y. Harayama et al. (2008) study was based purely on near-IR (NIR) photometry and included only stars with masses less than $20M_{\odot}$. Yet NGC 3603 is known to contain one of the largest collections of massive stars known in the Milky Way, with ~50 known O-type stars, including a dozen of the hottest and most luminous stars known (L. Drissen et al. 1995; N. W. Melena et al. 2008). The brightest star in NGC 3603 is designated A1 and is a double-line binary, with masses as high as any known in the Milky Way, $93M_{\odot}$ and $70M_{\odot}$ (P. Massey et al. 2025). Within the Local Group, only the R136 cluster may outstrip NGC 3603 in its massive-star content (e.g., A. F. J. Moffat et al. 1994; N. R. Walborn et al. 2014).

Given the large number of extremely massive stars known in NGC 3603, we thought that potentially it really might have a top-heavy IMF. Our earlier study (N. W. Melena et al. 2008) whetted our appetite, and we continued observing its brightest stars spectroscopically with the Magellan 6.5 m telescopes once that project had finished. The central cluster is very dense, and we were fortunate to have obtained time with the Hubble Space Telescope (HST) to obtain spectra of many of its most crowded stars. In this paper we use photometry from HST and ground-based imaging with newly obtained spectra to reanalyze the massive-star content of the cluster. In Section 2 we describe our observations and reductions, including the use of Gaia data to identify members. In Section 3 we present our spectral classifications and identify newly found binaries. We give our analysis in Section 4, presenting a color–magnitude diagram (CMD) and producing a reddening map. In Section 5 we construct the H-R diagram (HRD) after deriving physical properties from our new data and compare the stars' locations to evolutionary tracks. In Section 6 we derive the slope of the IMF. A summary of our work and a discussion of our results can be found in Section 7.

2. Observations and Reductions

2.1. Photometry

N. W. Melena et al. (2008) describe their photometry using archival HST images obtained with the High-Resolution Camera (HRC) of Advanced Camera for Surveys (ACS). The data had been taken through the F435W and F550M filters as part of program 10602 (PI: Jesús Maíz Apellániz) and had consisted of four dithered exposures, totaling 8 s in each of the two filters. N. W. Melena et al. (2008) had performed aperture photometry on the images, correcting the values for charge transfer efficiency losses, and transformed the photometry to the standard Johnson *B* and *V* system rather than remaining in the "native" ACS/HRC system. Complete details are given in Section 2.3 of N. W. Melena et al. (2008). We repeated their procedure here but used the point-spread-fitting program DAOPHOT (P. B. Stetson 1987) as implemented in IRAF[8] (D. Tody 1986, 1993; M. Fitzpatrick et al. 2024) rather than relying on just aperture photometry. For most stars in common with N. W. Melena et al. (2008) this resulted in negligible differences (<0.01–0.02 mag), with the values presented in their Table 1, but it allowed us to resolve a few stars that were blended in their study (e.g., NGC 3603-33). We also extended their photometry to slightly fainter stars, adding 16 stars by hand. Their study was also directed primarily at stars for which they had spectroscopic information, while our goal here is broader, namely to help characterize the entire massive-star population of the cluster. There are 213 stars with final photometry from the ACS/HRC data.

The ACS/HRC images covered only the small, crowded central region of NGC 3603, roughly 30″ on a side. To extend our coverage, we used data obtained with the 1.3 m telescope located on Cerro Tololo Inter-American Observatory (CTIO) taken with the ANDICAM imager built and operated by the SMARTS consortium. The CCD was a Fairchild 447 with a pixel scale of 0.″371 pixel^{-1} on the 1.3 m. The data were taken on (UT) 2008 January 22 in queue mode and consisted of 12 exposures: three 80 s *B*, three 20 s *B*, three 40 s *V*, and three 10 s *V*. The consortium delivered reduced, flat-fielded images that were 950 × 856 pixels, corresponding to 5.′9 (EW) by 5.′3 (NS), or 0.009 deg^2. The delivered image quality was 3.2–4.3 pixels (1.″2–1.″6) on the 12 images. We performed digital photometry through a 5-pixel (1.″9) radius aperture.

[8] NOIRLab IRAF is distributed by the Community Science and Data Center at NSF NOIRLab, which is managed by the Association of Universities for Research in Astronomy (AURA) under a cooperative agreement with the US National Science Foundation.

Table 1
Photometry and Spectroscopy of Stars Seen toward NGC 3603

ID[a]	R.A.$_{J2000}$	Decl.$_{J2000}$	V	V_{err}	$B-V$	$B-V_{err}$	Field[b]	Gaia Mem. Prob.	Spectroscopy		Comment
									Type	Reference	
2000	11:14:46.886	−61:16:00.63	10.78	0.00	0.23	0.00	2	0.000	⋯	⋯	HD306201
Sh 3	11:15:23.852	−61:15:01.34	11.06	0.00	0.21	0.00	2	0.000	A0V	(1)	HD306199
A1	11:15:07.305	−61:15:38.43	11.18	0.02	1.03	0.03	1	RUWE	O3If*/WN6	(4)	⋯
2001	11:14:47.746	−61:13:17.40	11.24	0.00	0.25	0.00	2	0.000	⋯	⋯	HD306198
B	11:15:07.411	−61:15:38.58	11.33	0.02	1.01	0.03	1	RUWE	O3If*/WN6	(4)	⋯
Sh 14	11:15:26.771	−61:17:48.40	11.65	0.00	0.16	0.00	2	0.000	⋯	⋯	⋯
C	11:15:07.589	−61:15:38.01	11.90	0.00	1.05	0.00	1	0.438	O3If*/WN6	(4)	⋯
2002	11:14:51.826	−61:12:49.51	12.10	0.00	1.19	0.00	2	0.000	⋯	⋯	⋯
Sh 9	11:15:15.157	−61:17:34.90	12.17	0.00	0.58	0.00	2	0.000	⋯	⋯	⋯
Sh 25	11:15:07.640	−61:15:17.53	12.33	0.00	1.50	0.00	2	1.000	B1Iab	(3)	⋯
2003	11:15:25.492	−61:18:03.31	12.37	0.00	0.18	0.00	2	0.000	⋯	⋯	⋯
201	11:14:44.159	−61:14:42.48	12.51	0.00	1.38	0.00	2	0.000	late	(4)	⋯
A2	11:15:07.313	−61:15:38.79	12.53	0.03	1.03	0.03	1	NoGaia	O3V((f))	(2, 4)	⋯

Notes.
[a] "Sh" designations are from D. Sher (1965). Double-digit designations are from A. F. J. Moffat et al. (1994). Letter designations came originally from W. H. van den Bos (1928), who visually identified several components in the central "nebulous star" CPD −60°2732, which were and further resolved by speckle (K. H. Hofmann & G. Weigelt 1986) and subsequently HST imaging (A. F. J. Moffat et al. 1994; N. W. Melena et al. 2008). All other designations (i.e., three or four digit numbers) are either from N. W. Melena et al. (2008) or new here.
[b] Field: 1 = ACS, 2 = ANDICAM.
References. For spectral types: (1) A. J. Cannon & M. W. Mayall (1949); (2) L. Drissen et al. (1995); (3) N. W. Melena et al. (2008); (4) this paper (some of which were reclassified from previous sources) based on newly obtained spectra. (5) A. Roman-Lopes (2013b) based on NIR spectra, and here based on newly obtained optical spectra.
(This table is available in its entirety in machine-readable form in the online article.)

Relative zero-point corrections were determined for the data taken in each filter, and the photometry was then averaged in a filter-by-filter manner. There were 757 stars in the final B catalog and 698 in the final V catalog, with 615 stars in common between the two.

Although we would like to adjust the zero-points of our ground-based data to those of the ACS/HRC photometry, there are two problems. First, the ACS/HRC photometry covers only a very small range of colors since nearly all the stars in the central cluster are O-type stars with similar reddening. Thus, we needed high-quality photometry in common with the ground-based data to determine what color terms, if any, to apply to our instrumental values. The second problem is that only one of the stars in the central cluster covered by the ACS/HRC images, Sh 50, is sufficiently isolated to make a reasonable comparison with our ground-based imaging. Thus, to set the zero-point for the ANDICAM data, we used the photoelectric photometry of S. van den Bergh (1978). These measurements were carried out for 23 of the brighter, least crowded stars identified by D. Sher (1965) in the NGC 3603 field and were obtained using a system that is a much closer match to the original *UBV* system than any CCD observations are likely to be. S. van den Bergh (1978) warns that the B-band photometry in particular might be contaminated by nebula emission, and so we restricted our determination of the zero-points to the brightest stars in his sample.

The resulting transformation equations showed no color term in V and a slight color term in B, $\sim 0.061 \times (B-V)$, fairly typical in our experience. When we applied this transformation to the ANDICAM data, we were pleased to find that both the ACS and ANDICAM photometry of Sh 50 yielded the same value for V, 14.72 (±0.03 for ACS, ±0.01 for ANDICAM), and that the agreement at $B-V$ was reasonable, with values of 1.14 ± 0.05 and 1.17 ± 0.01, respectively.

Finally, we eliminated all stars from the ANDICAM photometry that were in common with the ACS. This left 551 stars (from 609) added from the ANDICAM photometry to the final catalog, which contains 764 stars in total. We list these stars in Table 1, where we indicate whether the photometry comes from the ACS field or from the extended ANDICAM region. In identifying the stars, our preference was not to give new designations to those stars already in the literature. Thus, we generally retain the names provided by D. Sher (1965), K. H. Hofmann & G. Weigelt (1986), A. F. J. Moffat et al. (1994), and N. W. Melena et al. (2008), particularly in the case of stars with prior spectroscopy. For the remaining stars, we have added our own numbering, an extension of the numbers used in N. W. Melena et al. (2008). Stars with numbers of 2000 and above are all stars without spectroscopy, and the additional numbers are in order of decreasing brightness.

We confirmed that the ACS and ANDICAM photometry went equally deep. Both have a drop-off in their numbers at $V = 18$–18.5 and $B = 19$–19.5, several magnitudes deeper than we need, as we will show in Section 5.3.

During our work, we confirmed a significant shift from the ACS coordinate system to that of the standard ICRS system. We had calibrated our ground-based images using the ASTROMETRY.NET software (D. Lang et al. 2010). The offsets were $\alpha_{ACS} - \alpha_{ICRS} = +0.180$ s and $\delta_{ACS} - \delta_{ICRS} = -0\farcs21$. After applying this, we found that the coordinates derived from the ACS agreed with Gaia positions to roughly ±0.″05. The ANDICAM coordinates agreed with Gaia positions to roughly ±0.″2.

Stars with photometry are identified in Figures 1 (ACS) and 2 (ANDICAM).

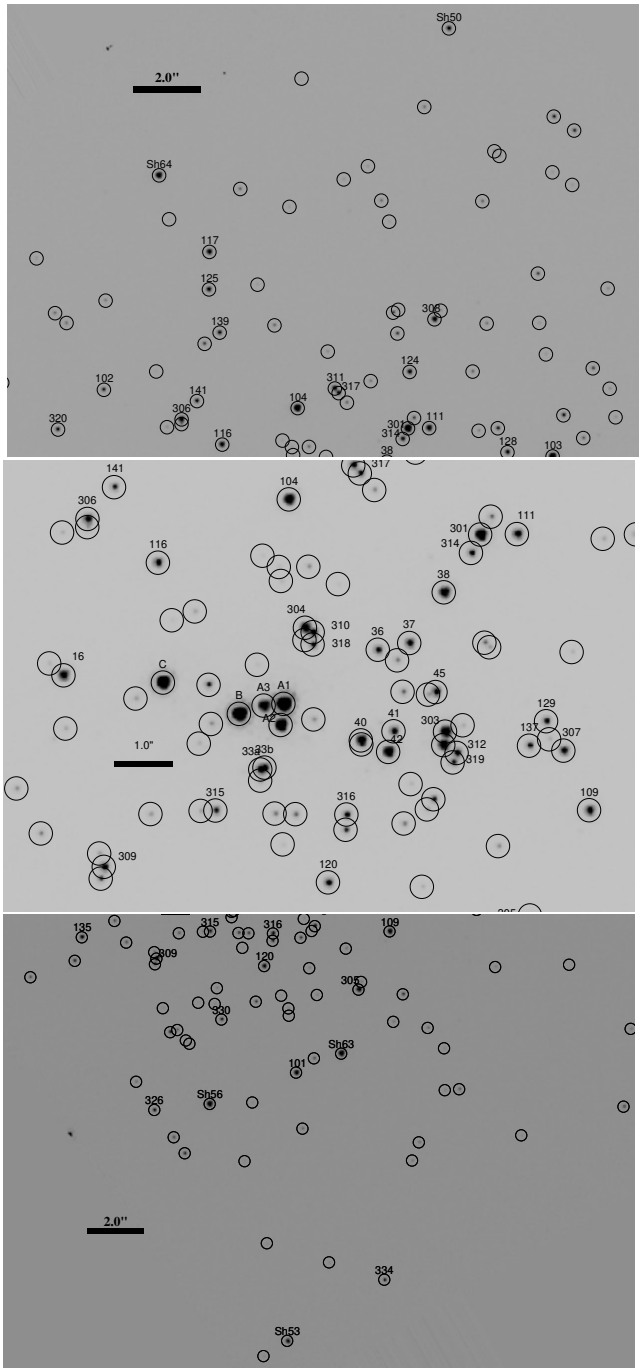

Figure 1. Program stars in the ACS field. Stars with photometry on the ACS fields are encircled; those that also have spectral types are identified with their designations from Table 1. The top panel is the northern portion of the ACS image; the bottom panel shows the southern portion. Each is roughly 16″ on a side. The middle panel shows the crowded central region at an expanded scale and covers roughly 6.″5 on a side. The circles all have diameters of 0.″2. The ACS image has been rotated such that north is at the top and east is to the left.

2.2. Membership Based on Gaia Proper Motions

We next utilize astrometric data from Data Release 3 (DR3; Gaia Collaboration 2022; Gaia Collaboration et al. 2023) of the Gaia satellite (Gaia Collaboration et al. 2016) to help determine membership. Of our 764 stars, we have identification of 612 sources (80.1%) in the DR3 that also contain parallax and proper-motion data. Of these, only 85 out of 213 ACS stars, or 40%, had Gaia data, as might be expected owing to crowding. The ACS scale is 0.″05 pixel^{-1}, with a spatial resolution <0.″115 for well-dithered exposures.[9] Although the ultimate goal for Gaia is similar resolution, currently the resolution for a single scan is 0.″23–0.″7, depending on the orientation.[10]

We identified 29 isolated stars for which we have OB-type spectra, and we use these to define the average proper motions in R.A. and decl. (pmRA and pmDEC), along with the intrinsic dispersion in these quantities, as well as the average parallax. We then performed a covariance analysis in order to assign normalized probabilities for membership. Although Gaia parallaxes are notoriously unreliable beyond 2 kpc, we expect nonmembers to be foreground and not background stars, given the cluster's distance of 7.6 kpc (N. W. Melena et al. 2008) and the fact that we are working with luminous OB stars. The mean proper motions derived from those 29 stars are pmRA $= -5.67$ mas yr^{-1} and pmDEC $= +2.07$ mas yr^{-1}, with an intrinsic dispersion of about 0.08 mas yr^{-1} in R.A. and 0.06 mas yr^{-1} in decl.. The mean parallax is 0.1323 mas. The results are about as expected: the analysis confirms that 80% of the stars in the ACS field with Gaia data are probable members, while only about 49% of the stars with Gaia data in the extended ANDICAM field are likely members.

The renormalized unit weight error (RUWE) is a quantity provided with the DR3 data for every star; a value less than 1.4 is taken as an indication that the astrometric solution was well behaved (see L. Lindegren et al. 2021, as well as the unpublished review by L. Pearce 2021[11]). We found that many of the stars in the crowded ACS field had values of RUWE considerably higher than this cutoff. For instance, A1, the brightest member of NGC 3601, located deep in the core (see the middle panel of Figure 1), has a RUWE value of 13.6. However, if we used 1.4 as our cutoff, the number of stars for which we could use Gaia data as indicative of membership would drastically decrease, from 612 to 479. We note that issues with the astrometric solutions are reflected in the uncertainties assigned to the proper motions, i.e., a star with a large RUWE value will also have large uncertainties in its astrometric properties, and thus our covariance analysis probability assignment should be valid, in general. The exceptions are stars with very large RUWE values, such as A1. In examining our initial membership probabilities, we found that the handful of spectroscopically confirmed members with low membership probabilities mostly had RUWE values > 2.6. Thus, we have decided, somewhat arbitrarily, to ignore the Gaia data for stars with RUWE values of 2.5 or greater, and so we note this in Table 1 with the notation "RUWE."

Two stars were initially missed in our photometry, NGC 3603-215 and NGC 3603-220. Both are crowded: 220 is just to the east of the much brighter star Sh 22, and 215 is just slightly southeast of Sh 58. Both have Gaia data suggesting that they are members, but their photometry is compromised by their close companions. We have kept them since both have carefully obtained spectra; each are of type O7V. We exclude them from the CMDs and the analysis of

[9] https://hst-docs.stsci.edu/acsihb
[10] https://www.cosmos.esa.int/web/gaia/science-performance
[11] http://www.loganpearcescience.com/research/RUWE_as_an_indicator_of_multiplicity.pdf

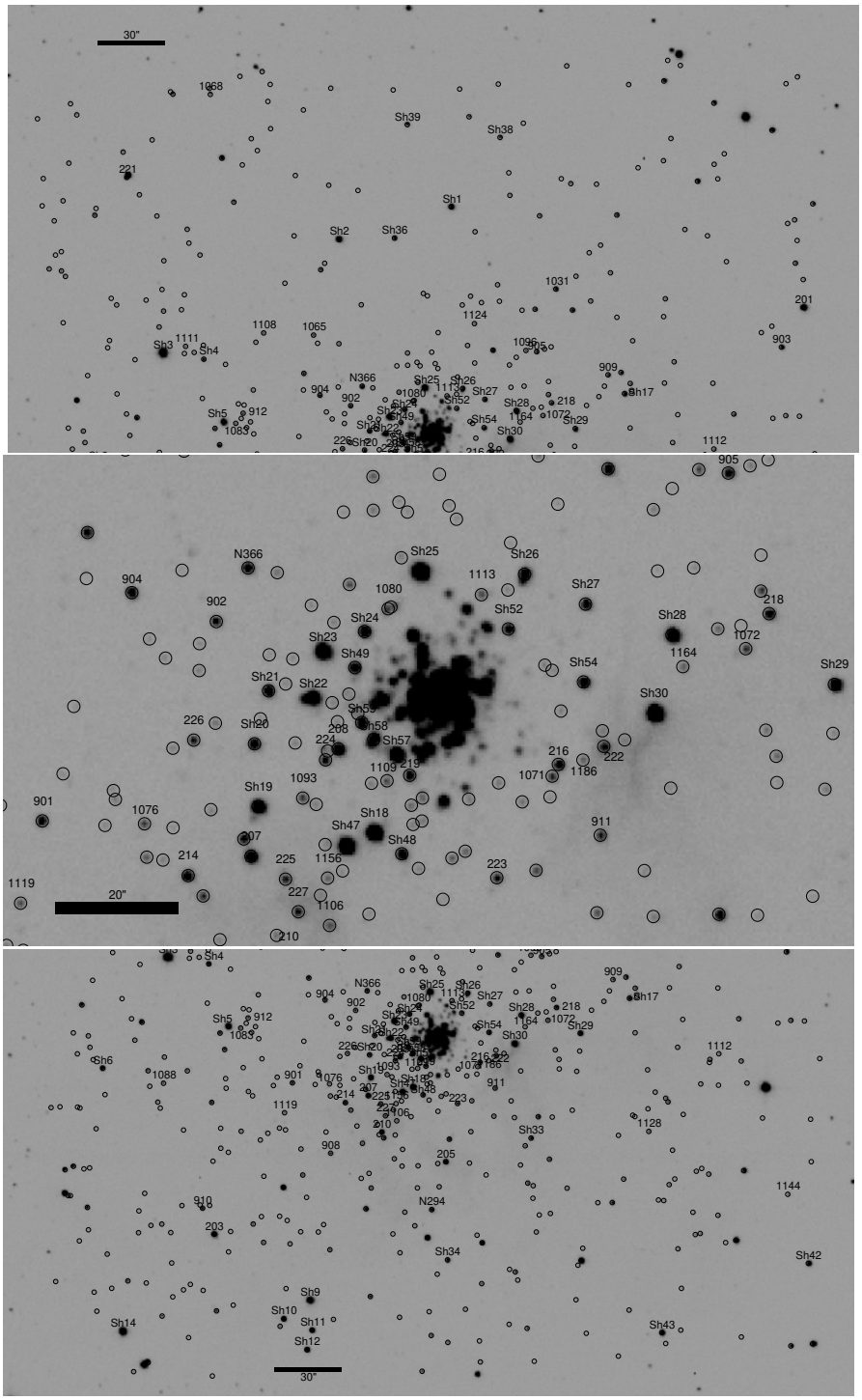

Figure 2. Program stars in the wider ANDICAM field. Stars whose photometry came from the ANDICAM data are encircled; those that also have spectral types are identified with their designations from Table 1. The top panel is the northern portion of the ANDICAM field; the bottom panel shows the southern portion. Each is roughly 6.′3 × 3.′3 on a side. The middle panel shows the more crowded region at an expanded scale and covers roughly 2.′3 × 1.′4 on a side. The circles all have diameters of 1.″0. The image used here is part of a *V*-band exposure obtained with the Swope 1 m.

color excesses in the following sections but retain them in the HRD.

2.3. Spectroscopy

L. Drissen et al. (1995) reported spectral types for 12 stars from data obtained with the Faint Object Spectrograph (FOS) on board HST. Their study primarily found O3-type stars, which are among the hottest and most luminous stars known, similar to what was found several years later in the R136 cluster by P. Massey & D. A. Hunter (1998). The L. Drissen et al. (1995) work piqued our interest in the cluster, and we began our own spectroscopic study. We reported spectral types for an additional 16 stars in N. W. Melena et al. (2008) using data from the Inamori Magellan Areal Camera and Spectrograph (IMACS; A. Dressler et al. 2011) on the Baade

Table 2
Spectroscopy Runs

UT Date	Instrument	Slit Width	Telescope	Disperser	Resolution	Coverage	Seeing
2006 Apr 12, 15[a]	IMACS f/4 long slit	0.″7	Baade	600/8.6	$\Delta\lambda = 2.0$ Å	3600–7000 Å[b]	0.″6–1.″1
2008 Apr 21–23	IMACS f/4 long slit	0.″7	Baade	600/8.6	$\Delta\lambda = 2.0$ Å	3600–7000 Å[b]	0.″5–1.″0
2008 Jun 14–16	IMACS f/4 long slit	0.″7	Baade	600/8.6	$\Delta\lambda = 2.0$ Å	3600–7000 Å[b]	0.″6–0.″9
2009 Mar 10, 12	IMACS f/4 long slit	0.″7	Baade	600/8.6	$\Delta\lambda = 2.0$ Å	3600–7000 Å[b]	0.″5–1.″0
2010 May 15, 16, Sep 5	STIS/CCD	0.″2	HST	G430M, G750M	$\Delta\lambda = 1.1$, 1.3 Å	4050–4845 Å, 6300–6860 Å	⋯
2010 Mar 22, Jul 10, Oct 30	STIS/CCD	0.″2	HST	G430M	$\Delta\lambda$ =1.1 Å	4310–4590 Å	⋯
2012 Feb 12, 13	MagE	0.″7, 1.″0	Clay	Fixed prism	$R = 4100$	3200–9500 Å	0.″5–0.″9
2021 Apr 21	MIKE	1.″0	Clay	Fixed R2.4	$R = 28{,}000$	3800–6100 Å	1.″5–2.″2
2021 Apr 22, 23	MIKE	0.″7	Clay	Fixed R2.4	$R = 40{,}000$	3800–6100 Å	0.″8–1.″3
2023 Feb 27	MagE	1.″0	Baade	Fixed prism	$R = 4100$	3200–9500 Å	0.″6–1.″0
2023 Feb 28	IMACS $f/4$ multislit	1.″0	Baade	1200/17.5	$\Delta\lambda = 1.3$ Å	3850–5150 Å	0.″7–0.″8

Notes.
[a] Included in N. W. Melena et al. (2008).
[b] Gaps in coverage occurred at 4410–4440 Å, 5200–5230 Å, and 6000–6030 Å.

6.5 m Magellan telescope at Las Campanas Observatory. Those data were taken in long-slit mode using a 0.″7-wide slit with the long focal length ($f/4$) camera and the 600 line mm^{-1} grating, yielding a spectral resolution of 2.0 Å and covering the wavelength region 3600–7000 Å. These were also mostly of very early O type, and we continued our spectroscopic investigation through 2023. We used the same IMACS setup to obtain spectra of additional NGC 3603 stars, as well as employing IMACS with multislit plates. Additional spectra were obtained using the Magellan Inamori Kyocera Echelle (MIKE; R. Bernstein et al. 2003) on the Clay 6.5 m Magellan telescope and the Magellan Echellette Spectrograph (MagE; J. L. Marshall et al. 2008) on either the Clay or the Baade, depending on the year. We also obtained spectra of the most crowded stars using the Space Telescope Imaging Spectrograph (STIS; B. E. Woodgate et al. 1998; E. Rickman & J. Brown 2024). We summarize our data sets in Table 2.

The biggest challenge facing spectroscopy of the NGC 3603 stars is crowding. The most crowded stars were observed as part of a Cycle 17 HST program using a 0.″2-wide slit. For the ground-based data, care was taken to observe crowded stars only in the best seeing and with slits widths of 0.″7. Less crowded stars were observed under worse conditions. Additional details are given below:

(1) The IMACS long-slit Magellan observations usually were taken with the slit oriented in such a way that two or more stars could be observed simultaneously. The 0.″7-wide slit covers nearly 15′ in length, providing much flexibility in our choice of targets. Since the instrument has an atmospheric dispersion corrector (ADC), this could be done with little loss of flux even at the blue end. The detector consists of a mosaic of eight 2 K × 4 K CCDs arranged in two rows (i.e., 8 K × 8 K in total), resulting in wavelength gaps unless two grating tilts are used. For the long-slit observations (2006–2009), we instead were simply careful in our setup to assure that no critical lines fell into these gaps. Given the fine spatial sampling of the unbinned CCDs (0.″11) and a best focus of 5 unbinned spectral pixels with the 0.″7-wide slit, we operated the detector in a 2 x 2 binned mode. Flat-field observations were obtained in the afternoon for removing pixel-to-pixel variations, and a HeNeAr comparison lamp was obtained after each observation for wavelength calibration.

(2) STIS/CCD HST observations were made under program GO-11626 (PI: Massey), utilizing 28 orbits during six visits in Cycle 17, with the explicit purpose of addressing the high-mass end of the mass function. The goal was to obtain spectral classification of the stars that were too crowded to observe from the ground in the core of the cluster. The 11 brightest stars were observed with four grating settings: G430M/4194, G430M/4451, G430M/4706, and G750M/6581. The three G430M grating settings provided continuous coverage from 4050 to 4845 Å, a region that contains the spectral lines most critical for classification, while the G750M observation covered the Hα line. At each grating setting, the star was dithered to five positions along the 0.″2 × 52″ slit, with steps of 0.″5 in order to reduce the effects of hot pixels and cosmic rays. In addition, the longer exposures (typically > 270 s) were also CR-SPLIT at each dither point. An additional 25 stars were observed with just the critical G430M/4451 setting. This region included Hγ and the temperature-sensitive He I λ4471 and He II λ4542 lines, on which the classification of O-type stars is based (P. S. Conti 1973; N. R. Walborn & E. L. Fitzpatrick 1990; A. Sota et al. 2011). Observations were all made by using offsets from Sh 23, a carbon-rich O-type supergiant (OC 9.7Ia) with $V = 12.7$. The standard pipeline reductions were used up through wavelength calibration and flat-fielding, with the final extraction done using IRAF on the pipeline "flt" files in order to utilize optimal extraction techniques (see, e.g., P. Massey & M. M. Hanson 2013). A small, ±3-pixel aperture was used to extract each spectrum, with a modal background subtracted using regions on either side of the star. The extracted spectra were traced in the spatial direction. For the 11 bright stars with five dither positions, the spectra were then combined using the "avsigclip" algorithm; this resulted in vastly cleaned spectra. The final spectra of the three blue regions were then combined and the spectrum classified.

(3) MagE Magellan observations were made in 2012. Crowded stars were observed with the 0.″7 slit when the seeing was excellent (0.″5–0.″6). When the seeing was not quite as good, we switched to the 1″ slit and observed less crowded

stars. Calibration and data reduction relied on a combination of MTOOLS routines (written by Jack Baldwin) and IRAF echelle tasks, as described in P. Massey et al. (2012).

(4) MIKE Magellan observations were made during the first half of three nights in 2021 April. The seeing was particularly atrocious on the first night, requiring a wider slit (1″) than we preferred, but improved significantly for the next two nights, during which we used the 0.″7 slit. MIKE had recently been outfitted with an ADC, but it became clear from the first few observations that it was misaligned, and it was not used during the run. Flat-field observations were obtained during the afternoons by the use of a diffuser, and a ThAr exposure was obtained at 1 hr intervals for wavelength calibration. The data reduction used the same combination of MTOOLS and IRAF echelle routines previously mentioned.

(5) Both MagE and IMACS Magellan observations were made during 2023 February. As we shall see shortly, we had mostly found O-type stars, presumably of high masses. Our goal for this run was to go fainter, reaching down to B-type dwarfs. Our initial plan was to use both nights for IMACS observations with multislit plates. However, we learned upon our arrival that there were intermittent electronic failures rendering the use of chips c1–c4 problematical. Flat-field exposures through our masks during the afternoon, however, confirmed that the science targets all fell on chips c5–c8. Unfortunately, the alignment stars, needed for adjusting the mask in x and y, as well as rotation, were distributed throughout all eight chips, and the alignment routines required the software to be able to examine all eight chips. Dr. Carlos Contreras was kind enough to modify these routines in real time, despite being off-shift. We had difficulties with the alignments on the first night (due to user error on the part of PM) and switched to MagE to observe stars that did not fall on a mask. On the second night we observed all three masks, with the grating tilt adjusted between exposures in order to fill in the gaps. (Where a particular spectral line would fall depended on the spatial location of the slit on the mask, and this process assured that no critical line would be lost.) Each mask was observed for 3 x 1200 s at each of the two grating tilts, with HeNeAr comparisons and flat-field exposures done on-sky for each tilt. The data were reduced using the COSMOS3 software with aid from Drs. Gus Oemler and Daniel Kelson, who helped us deal with the fact that half the array was missing from the data. Altogether, 33 spectra (including some repeats) were obtained using three multislit masks.

3. Spectral Classification

Stars were classified by referring to the spectral atlases of N. R. Walborn & E. L. Fitzpatrick (1990), N. R. Walborn et al. (2002), and A. Sota et al. (2011), with additional reference to R. O. Gray & C. J. Corbally (2009) for the scant number of B-type stars and later. For stars observed only with HST, with its limited wavelength coverage, we measured the ratios of the equivalent widths of the He I λ4471 and He II λ4542 lines and used the quantitative classification criteria of P. S. Conti (1973), with luminosity classes assigned based on brightness. The latter readily distinguishes O supergiants from dwarfs but may confuse bright giants with the former and faint giants with the latter. We list these spectral types in Table 1 and identify those stars for which we have spectroscopy by their designations in Figures 1 and 2.

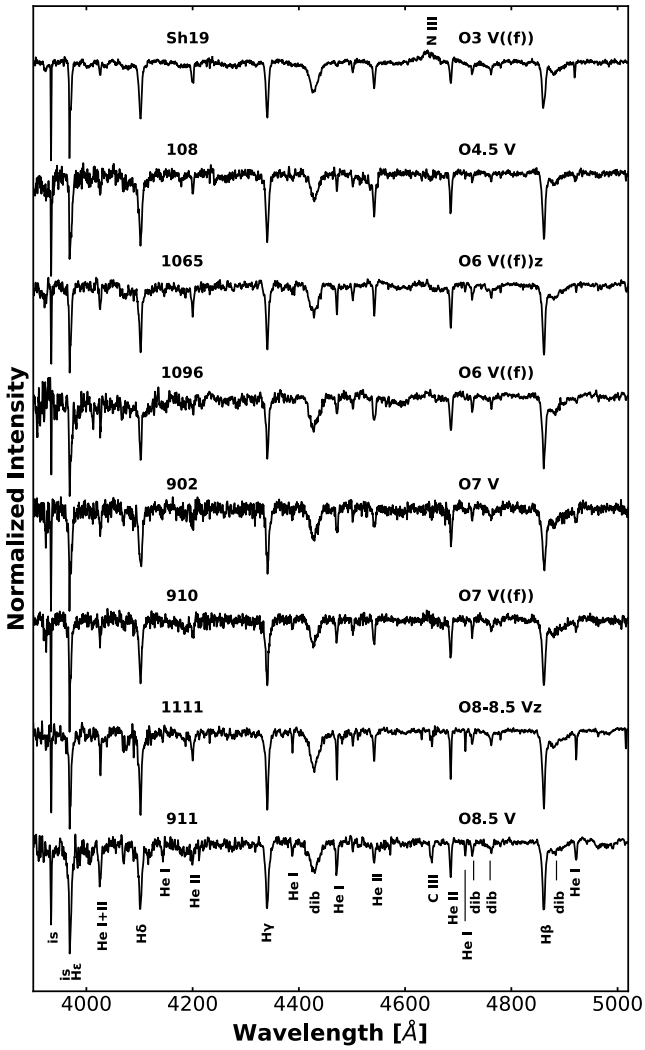

Figure 3. Representative spectra for early to mid-O. The spectra have all been normalized. We label each with its name and the adopted spectral types from Table 1. The principal spectra features are identified at the bottom, with both interstellar (is) lines and diffuse interstellar bands (dib) noted.

In Figures 3 and 4 we show representative examples of our spectra. The data have been normalized, and we have identified the principal spectral features.

3.1. O2-3If*/WN5-6 Stars and Other Stars from the Literature

Certain classifications require more discussion. The most luminous stars in young, highly populated clusters, such as NGC 3603, R136 in the LMC, and NGC 604 in M33, have spectral characteristics that are intermediate between the hottest O-type supergiants (O2-3.5If*) and mid-excitation WN-type Wolf–Rayet stars (WN5-6). N. R. Walborn (1982) introduced the notation O3If*/WN6 to describe the star Sk $-67^{\circ}22$ in the LMC. Such stars are often referred to as "slash" stars (e.g., P. S. Conti & B. Bohannan 1989), or characterized as "Of stars on steroids" (P. Massey & D. A. Hunter 1998). These are unlike normal WN stars, in that they are hydrogen-rich, possess absorption lines, and are much more luminous. They are now understood to still be in the hydrogen-burning phase (A. de Koter et al. 1997; P. Massey & D. A. Hunter 1998) and show WN-like emission lines simply because they are so close to their

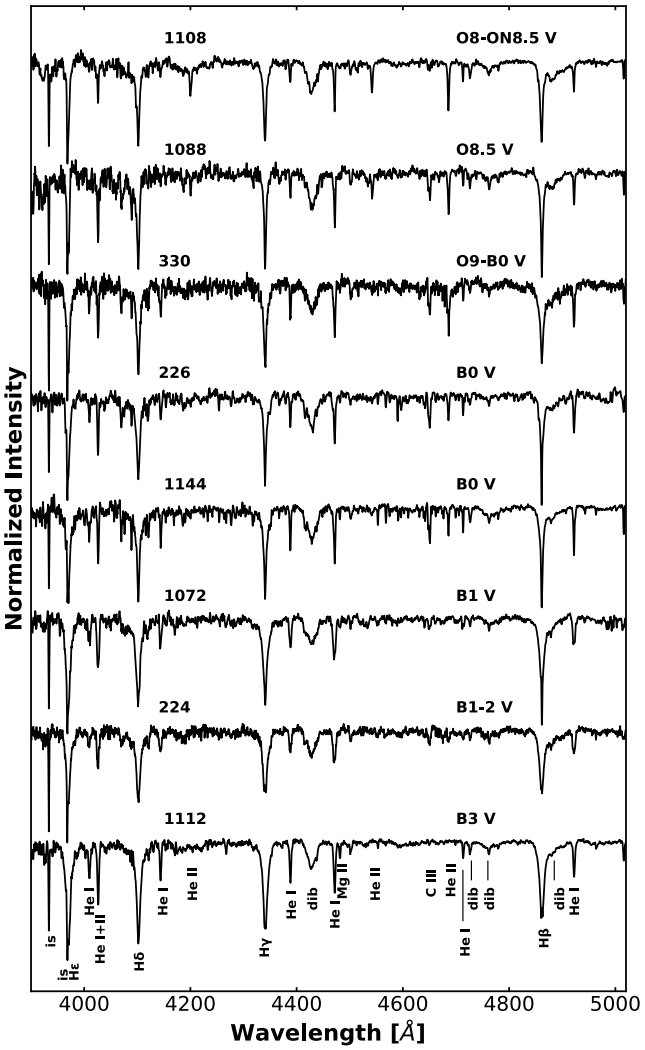

Figure 4. Representative spectra for mid-O to early B. The spectra have all been normalized. We label each with its name and the adopted spectral types from Table 1. The principal spectra features are identified at the bottom, with both interstellar (is) lines and diffuse interstellar bands (dib) noted.

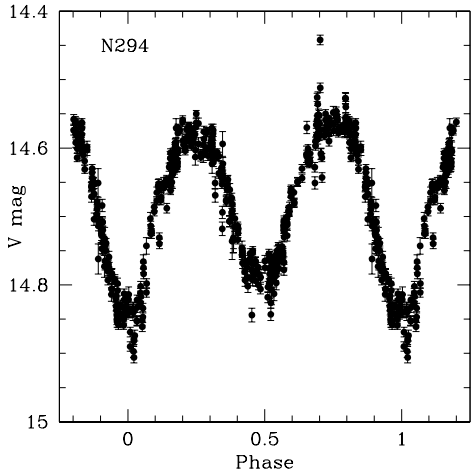

Figure 5. Light curve of N294. The data were collected in queue mode between 2006 January and 2007 June on the Yale 1 m telescope on Cerro Tololo as part of the SMARTS program. The data have been phased with a period of 1.93557440 days and a phase zero-point T0 of 2453758.374.

Eddington limit that their stellar winds are optically thick (P. A. Crowther & L. Dessart 1998; G. Gräfener et al. 2011; P. A. Crowther et al. 2012). N. W. Melena et al. (2008) did not have new spectra of their own of NGC 3603-A1, B, or C and simply quoted the "WN6+abs" types given by L. Drissen et al. (1995) based on optical HST/FOS spectroscopy. Examining their spectra today, we would call these all O3If*/WN6, and we have revised their types accordingly in Table 1. The star A1 is actually an O3If*/WN5-6 pair of stars; its primary has the highest mass known from a direct Keplerian measurement (A. F. J. Moffat & V. S. Niemela 1984; O. Schnurr et al. 2008; P. Massey et al. 2025).

A. Roman-Lopes (2012, 2013a) reports discoveries of two additional "slash" stars in NGC 3603, each classified as O2If*/WN6 on the basis of NIR spectroscopy. The first of these A. Roman-Lopes (2012) designates as WR42e; it is the star we call 903. A. Roman-Lopes (2012) suggests that it has been ejected from the cluster core since it is located in the outer region of the cluster. He notes that the ground-based proper motions are ambiguous on this issue. Our optical spectrum shows the star to be an O4Ifc. We can exclude the O2If*/WN6 classification on a number of grounds. First, He I λ4471 is clearly present; its strength relative to that of He II λ4542, along with the appearance of the rest of the spectrum, is consistent with an O4 type. Although He II λ4686 is in emission, its equivalent width is -5 Å, what we would expect of an O-type supergiant, but not of a WN star. Finally, although N IV λ4058 is in emission, its strength relative to N III $\lambda\lambda$4634, 42 is like that of other O4If stars. The "c" is added simply to denote that the carbon lines are strong.

As for NGC 3603-903 having been ejected from the cluster's core: its Gaia DR3 proper motion is in excellent agreement with that of the cluster as a whole, i.e., pmRA $= -5.679 \pm 0.02$ mas yr^{-1} and $+1.908 \pm 0.02$ mas yr^{-1}, compared to that of the cluster quoted above, pmRA $= -5.67$ mas yr^{-1} and pmDEC $= +2.07$ mas yr^{-1}, with intrinsic dispersions of 0.08 and 0.06 mas yr^{-1}, respectively. We note that our study has found lots of other early-type stars this far from the cluster core; one may reasonably assume that they formed there.

The second of these slash stars, referred to as MTT 58 by A. Roman-Lopes (2013a),[12] is the star we call N294. From the NIR spectrum, he arrives at an O2If*/WN6 spectral type for the dominant star. Its strong X-ray luminosity suggests that it is a close binary, and a careful inspection of their spectra led them to conclude that the companion is an O3If*. Using SMARTS data obtained in the Yale 1 m CTIO telescope in 2006 and 2007, we had already identified the star as a 1.94-day contact binary; its light curve is shown in Figure 5. We continued to obtain Magellan optical spectra in order to determine an orbit solution for this massive pair. We agree with the O2If*/WN6+O3If* classification of A. Roman-Lopes (2013a). We will describe the data and perform the orbital analysis in a subsequent paper, where we will discuss several other massive binaries in the NGC 3603 cluster.

A third massive star has been classified spectroscopically since N. W. Melena et al. (2008): also an X-ray source, the star is called MTT68 by J. Melnick et al. (1989) and was classified as O2If* by A. Roman-Lopes (2013b), also using NIR spectroscopy. It is listed as 1031 in our Table 1. However,

[12] The designation is from J. Melnick et al. (1989).

our optical spectra suggest an O3If spectral type. We find that N IV λ4058 is stronger than N III λ4634, 42, but not to the extent demanded for the O2 classification (N. R. Walborn et al. 2002).

3.2. Binaries

In the previous subsection we discussed the binaries A1 (O3If*/WN6+O3If*/WN5; P. Massey et al. 2025) and N294 (O2If*/WN6+O3If*; A. Roman-Lopes 2013a). Here we list what we know about other identified binaries in the NGC 3603 cluster.

Sh 56. This star was classified as "O3III(f)+O?" by N. W. Melena et al. (2008). We obtained a second spectrum of the star with IMACS on 2008 June 14 (see Table 2). Many of the He I and He II lines are double. Thus, we confirm the fact that the star is composite, but we cannot improve on the N. W. Melena et al. (2008) classification.

207. We identified this star as an eclipsing binary as part of our SMARTS project, with a period of 1.07192 days. There are two equally deep (0.4 mag) eclipses. We classify the star here as "O7V+O8V" based on a series of 10 spectra we obtained between 2008 April 21 and 2010 February 23. It is also listed in N. Mowlavi et al. (2023) as a Gaia-detected eclipsing binary. We believe that this system deserves spectroscopic follow-up.

37. The star was classified as "O6.5+OB?" by L. Drissen et al. (1995). We have no additional information about this system, and we adopt their spectral type here.

Sh 49. We identified this as an eclipsing binary as part of our SMARTS project, with a period of 1.4858 days and 0.2–0.4 mag eclipses. The star was classified as "O7.5V" by N. W. Melena et al. (2008). We have 10 spectra taken with IMACS and MagE between 2009 February 14 and 2012 February 13. We see variations in the line profiles and radial velocity variations of order 250 km s^{-1} but no sign of double lines.

Sh 4. We classify this star as possibly composite ("O3.5IIIf + bin?"), as the spectral energy distribution (SED) turns up at wavelengths above 5000 Å, and the strength of He I λ5876 is much greater than one would expect given its minimal presence at λ4471. Our guess would be that the companion is an early B-type star.

N366. This was also identified as an eclipsing binary as part of our SMARTS project with a period of 1.6113 days and shallow eclipses (0.05–0.10 mag). We have 11 Magellan spectra (IMACS and MagE) taken between 2008 April 22 and 2012 February 13. We do not measure any significant radial velocity variations, nor do we detect any double lines.

223. We classify this as B0.3III+early B, as some of the spectral lines (e.g., He I λ4471) are double. Si IV is not.

In addition, our modeling effort (Section 5.1.1) failed to find acceptable fits for two stars: Sh 18 and 208. That leads us to suspect that each of them is composite.

4. Analysis

4.1. Color–Magnitude Diagram

In the previous sections we presented our photometry, determined the probability of membership based on Gaia proper motions, and described our spectroscopy. In Figure 6 we combine these data in a CMD to get a more accurate assessment of the stellar content of the cluster and the limitations of determining the IMF.

The red symbols denote stars whose Gaia data suggest that they are not members (normalized probability < 0.5 from Table 1). Black is used for stars whose Gaia data suggest that they are members, while cyan is used for stars lacking adequate Gaia data (i.e., no proper motions or RUWE $\geqslant 2.5$). Spectroscopically confirmed members are shown as filled circles.

We see that in general the cluster members occupy a color range from a $B - V \sim 0.9$ to a $B - V \sim 1.7$, with foreground stars (red symbols) mostly occupying a diagonal band stretching from the brightest, bluest magnitudes ($V \sim 11$, $B - V \sim 0.2$) to where they merge with the cluster at $V \sim 17$, $B - V \sim 1.0$.

For the most part, there is excellent agreement between the results of our spectroscopy and the Gaia proper motions once stars with high RUWE values have been ignored. The stars assigned to be members on the basis of Gaia data that also have spectroscopy indicating they are members are shown by black circles; there are 71 such stars.

Similarly, there are six stars, shown by red crosses in Figure 6, where both the Gaia data and spectroscopy demonstrate nonmembership. Four of these (Sh 1, Sh 2, NGC 3603-201, and NGC 3603-203) are bright and fall into the color range $B - V = 0.9$–1.4 where we expect to find members, but our spectroscopy shows that these are late-type stars, in accord with their Gaia data. A fifth example is Sh 3 (HDE 306199), the second-brightest star, shown by the red cross in the upper left of the CMD. This was identified as an A0 star in the Henry Draper Extension (A. J. Cannon & M. W. Mayall 1949) and is certainly not a member. A sixth star, NGC 3603-225, is confirmed as a late-type star in agreement with Gaia nonmembership, despite its colors; it is much fainter ($V = 15.68$) than the other five, near the limits of our spectroscopy.

There are two stars, indicated by red circles, whose Gaia data suggest that they are nonmembers, but whose spectroscopy proves otherwise: NGC 3603-C (O3If*/WN6) and NGC 3603-38 [O3.5V((f))]. There is no question of actual membership, and both of these stars are in the crowded center. Their RUWE values are 1.6 and 2.1, both indicative that the Gaia data are unreliable, but below our more generous cutoff of 2.5. There are no stars whose Gaia data indicate membership but this is contradicted by our spectroscopy.

There are, of course, many stars without complete data. There are 159 stars with neither reliable Gaia data nor spectroscopy, shown by cyan triangles. For these stars, we can only go by their locations in the CMD to guess membership. There are 211 stars, shown by black triangles, whose Gaia data suggest that they are members but that lack spectroscopy. A few of these are found outside the color range in which we expect to find members; either their photometry or their Gaia data are likely off.

A comparison of the figure with the data in Table 1 shows that the identification of cluster members is increasingly muddled at magnitudes fainter than $V = 16.5$. We find that by $V \sim 17$ Gaia is identifying a few stars as cluster members that are likely too blue to belong to the cluster. Worse, however, is

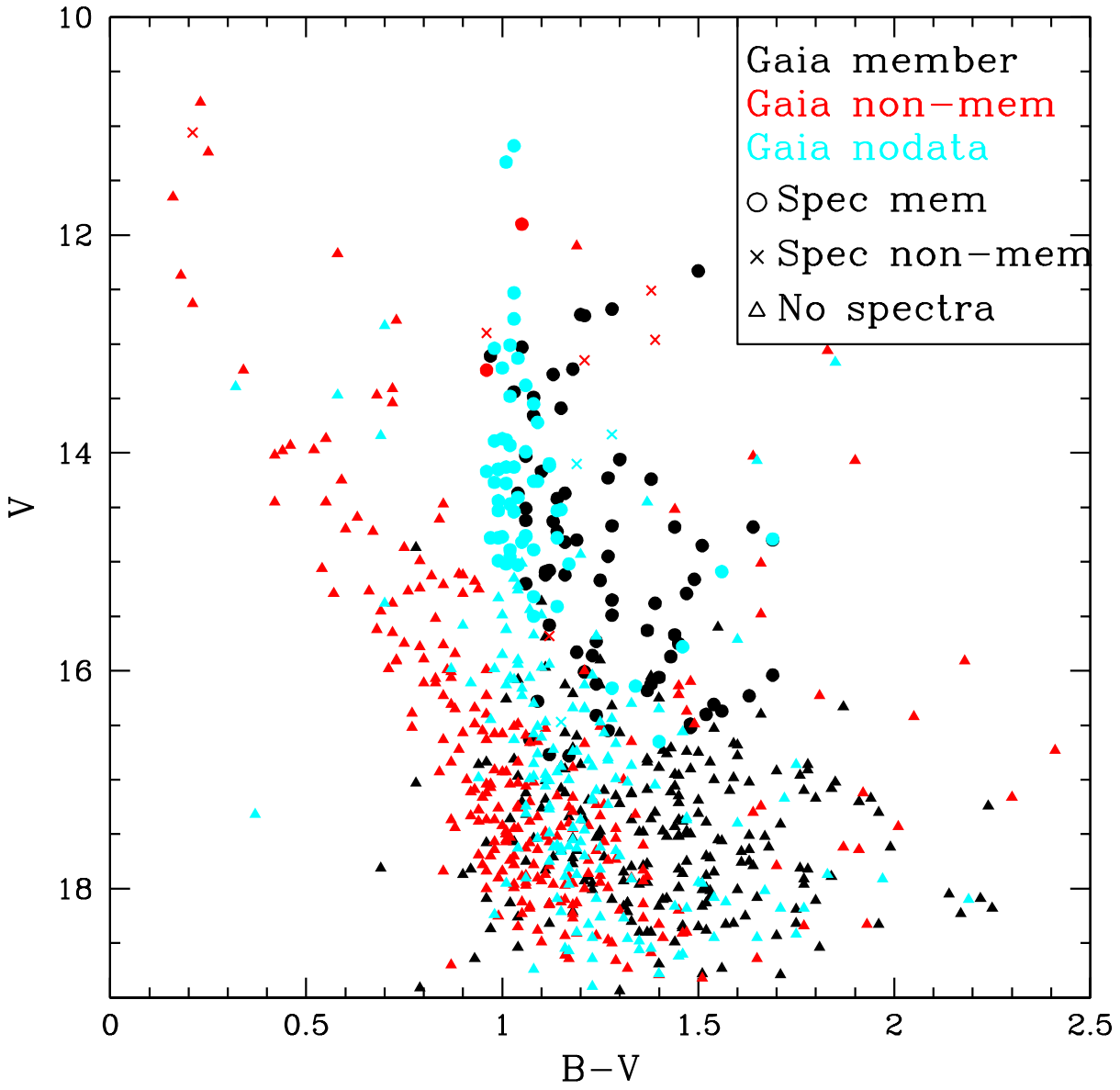

Figure 6. CMD for NGC 3603. As denoted in the legend, Gaia members are marked in black, Gaia nonmembers in red, and stars without reliable Gaia data in cyan. Circles denote stars shown by spectroscopy to be members, crosses denote stars confirmed to be nonmembers by spectroscopy, and triangles indicate stars without spectroscopy. There is a large swath of Gaia nonmembers extending from the brightest, bluest stars down to where cluster members are found at $V \sim 17$, $B - V \sim 1.0$. Cluster members mostly occupy a color range of $0.9 < B - V < 1.7$.

the mixture of a large sample of stars without good Gaia data and probable members and nonmembers at $V = 17$. Our spectroscopy becomes increasingly incomplete below $V = 16$, as is readily apparent from a comparison with Table 1. The faintest stars with spectroscopy are a couple of B dwarfs at $V = 16.8$; our spectroscopy is relatively complete above $V = 16.0$. Further spectroscopy is clearly needed at $V > 16$ within the expected color band ($0.9 > B - V < 1.7$), but what can we answer from the copious data in hand?

One further complication we can infer from the CMD is that the extinction is not uniform within the cluster. To a good approximation, all the spectroscopically confirmed stars will have the same intrinsic colors, to within 0.05 or less in $B - V$. Yet the colors of the cluster members at $V = 15$ extend from $B - V \sim 1.0$ to 1.7. N. W. Melena et al. (2008) found $(B - V) \sim 1.4$ with little variation across the cluster core (in agreement with previous studies), which would correspond roughly to $E(B - V) = 1.2$, consistent with where a majority of the members in the CMD are found. We reexamine this issue in the following section.

4.2. Reddening

Within the cluster core, N. W. Melena et al. (2008) adopt a two-component model for the ratio of selective to total extinction, R_V, following the comprehensive study of A. K. Pandey et al. (2000), who adopted the standard $R_V = 3.1$ for a foreground reddening of $E(B - V) = 1.1$ and a value of $R_V = 4.3$ for color excess above that, i.e., $A_V = 3.41 + 4.3[E(B - V) - 1.1]$. N. W. Melena et al. (2008) found this consistent with their spectroscopic parallaxes (i.e., M_V computed from the dereddened photometry) compared to that expected for their spectral types if a distance of 7.6 kpc was adopted. N. W. Melena et al. (2008) show that this

distance is consistent with the kinematic distance to the cluster (see their Table 5 and discussion in their Section 4).[13]

There have been several pertinent studies over the following years based on analysis of the gas. X. Pang et al. (2016) used archival HST/WFC3 images to determine a pixel-to-pixel distribution of the color excess $E(B-V)$ of the gas based on the Hα-to-Paβ flux ratio within the central $2\farcm4 \times 2\farcm1$ region of the cluster, finding $E(B-V)$ ranging from 1.5 to 2.2 mag, although, as they note, this value represents an upper limit to the reddening of the associated stars since only some of the gas will be in front of the stars. A more recent study with JWST by C. Rogers et al. (2024) also measured the color excess and R_V value using recombination lines of the gas, finding $R_V = 4.8 \pm 1.1$ but a color excess corresponding to $E(B-V) = 0.64 \pm 0.3$. Such a low value is inconsistent with what we know of the reddening from stars (e.g., A. K. Pandey et al. 2000; N. W. Melena et al. 2008 and references therein).

Using our extensive spectroscopy, we can reexamine the issues of the extinction and the distance here. We begin by determining the color excesses $E(B-V)$ as a function of position within the cluster. The use of O-type stars for this is ideal, as their temperatures are so high that there is little variation in intrinsic color with spectral subtype. For this exercise we adopt the $(B-V)_0$ colors of F. Martins & B. Plez (2006) based on the SEDs computed with CMFGEN models by F. Martins et al. (2005). We note that their analysis results in $(B-V)_0$ colors about 0.04 mag redder than the commonly used values (see M. P. Fitzgerald 1970; A. N. Cox 2000) but are likely more accurate, as older values are based on higher surface gravity models than realistic (see discussion in F. Martins & B. Plez 2006). According to these studies, all O stars have an intrinsic color of -0.27 ± 0.01, with the exact value dependent on spectral subtype and luminosity class. We ignored the handful of stars with spectral types later than B1 and adopted $(B-V)_0 = -0.19$ for the B1Iab star Sh 25 (M. P. Fitzgerald 1970) and -0.26 for the B0−1V classes. We also ignored the O3If*/WN6 stars, as their colors will be affected by their strong emission lines.

We show a smoothed reddening map in Figure 7. We see at once that the cluster center has by far the lowest reddening values, with values generally increasing from $E(B-V) \sim 1.2$ (deep purple) to $E(B-V) \sim 2.0$ (light yellow). The obvious interpretation is that the strong stellar winds of the myriad of hot, luminous stars have blown a hole in the gas. This impression is confirmed by the visual appearance of the cluster in Hα and O III shown in the bottom panel of the figure. We will discuss the age of the cluster in more detail in the following section, but with the presence of so many short-lived O3I*/WN6 and O3 stars, the age must be close to 1–3 Myr. Hence, this clearing has taken place in a remarkably short time.

5. The H-R Diagram

We have already noted that there is only a negligible difference in the intrinsic $(B-V)_0$ colors of O-type stars, regardless of whether they are early-type O stars with effective temperatures of 45,000–50,000 K or late-type O stars with effective temperatures of "only" 30,000 K. This degeneracy of intrinsic colors with effective temperature is due to the fact that the flux in such stars peaks in the far-UV and there is little change in the slope of the tail of the Rayleigh–Jeans distribution. This degeneracy extends even into the near-UV colors; see examples and discussion in P. Massey (1998). Yet over this same range in temperature the visual bolometric correction changes by 1.5 mag, or a factor of 4 in luminosity. The mass–luminosity relationship is fairly flat for such high-mass stars: we calculate that $L \sim M^{1.9}$–$M^{2.2}$ near the zero-age main sequence (ZAMS) of the $Z = 0.014$ Geneva evolutionary tracks (S. Ekström et al. 2012), with the smaller exponent appropriate to the highest masses. Thus, an error of a factor of 4 in luminosity translates into an error of a factor of 2 in mass, which is significant if our interest is in measuring mass functions.

It is for this reason that we have relentlessly pursued our spectroscopic survey of the NGC 3603 stars. The optical spectrum is quite sensitive to the effective temperature, and the bolometric correction is easily computed from that temperature.[14] Combined with the absolute visual magnitude M_V (which, of course, depends on a knowledge of the distance and a correction for interstellar reddening), this allows us to compute an accurate luminosity, which can be used with evolutionary tracks to approximate the star's mass.

Of course, we do not have spectral types for all the stars in our sample, despite the many years of observations reported here. In this section we will lay out how we obtained effective temperatures and bolometric luminosities for the stars both with and without spectroscopy.

5.1. Stars with Spectroscopy

For an accurate placement in the HRD we need both the effective temperatures and the bolometric luminosities. For the stars with spectra, we can either obtain effective temperatures ($T_{\rm eff}$) by modeling the spectra or infer $T_{\rm eff}$ simply from the spectral classifications. To obtain the luminosities, we compute the absolute visual magnitude

$$M_V = V - A_V - 14.40,$$

where 14.40 is the true distance modulus corresponding to a distance of 7.6 kpc. The correction for interstellar extinction A_V is determined from the color excess $E(B-V)$ using the two-component model

$$A_V = 3.41 + 4.3[E(B-V) - 1.1],$$

[13] D. Weßmayer et al. (2023) derive a distance of 6250 ± 150 pc using Gaia parallaxes for 10 stars located near the core. This shorter distance was derived by excluding another 12 stars whose early O types clearly indicate membership (e.g., their Table B-1) and whose proper motions indicate near-certain membership by our own analysis here. Doubtless the N. W. Melena et al. (2008) distance determination will not be the last word on this subject, but we adopt their value since it agrees with the kinematic distance to the cluster. We note that the difference would amount to ∼0.5 mag in the distance modulus, which we believe would be hard to reconcile with the expected absolute magnitudes. We refer the reader to the recent analysis of the double-lined binary NGC 3603-A1, which found an absolute magnitude of the system $M_V = -7.3$, in agreement with the $M_V = -7.3$ value derived using the 7.6 kpc distance. To reconcile this with the 6.3 kpc distance would require stellar radii inconsistent with the light curve.

[14] From their FASTWIND analysis of LMC OB stars, P. Massey et al. (2005) proposed that a good approximation for the bolometric correction (BC) is $\mathrm{BC} = -6.90 \log T_{\rm eff} + 27.99$. Using CMFGEN models computed with solar metallicities, F. Martins et al. (2005) proposed instead $\mathrm{BC} = -6.80 \log T_{\rm eff} + 27.58$. The two approximations agree to within 0.06 mag over the range $T_{\rm eff} = 20{,}000$–$50{,}000$ K. Since CMFGEN includes a more exact treatment of blanketing and is based on a more appropriate metallicity for NGC 3603, we adopt the latter relationship here.

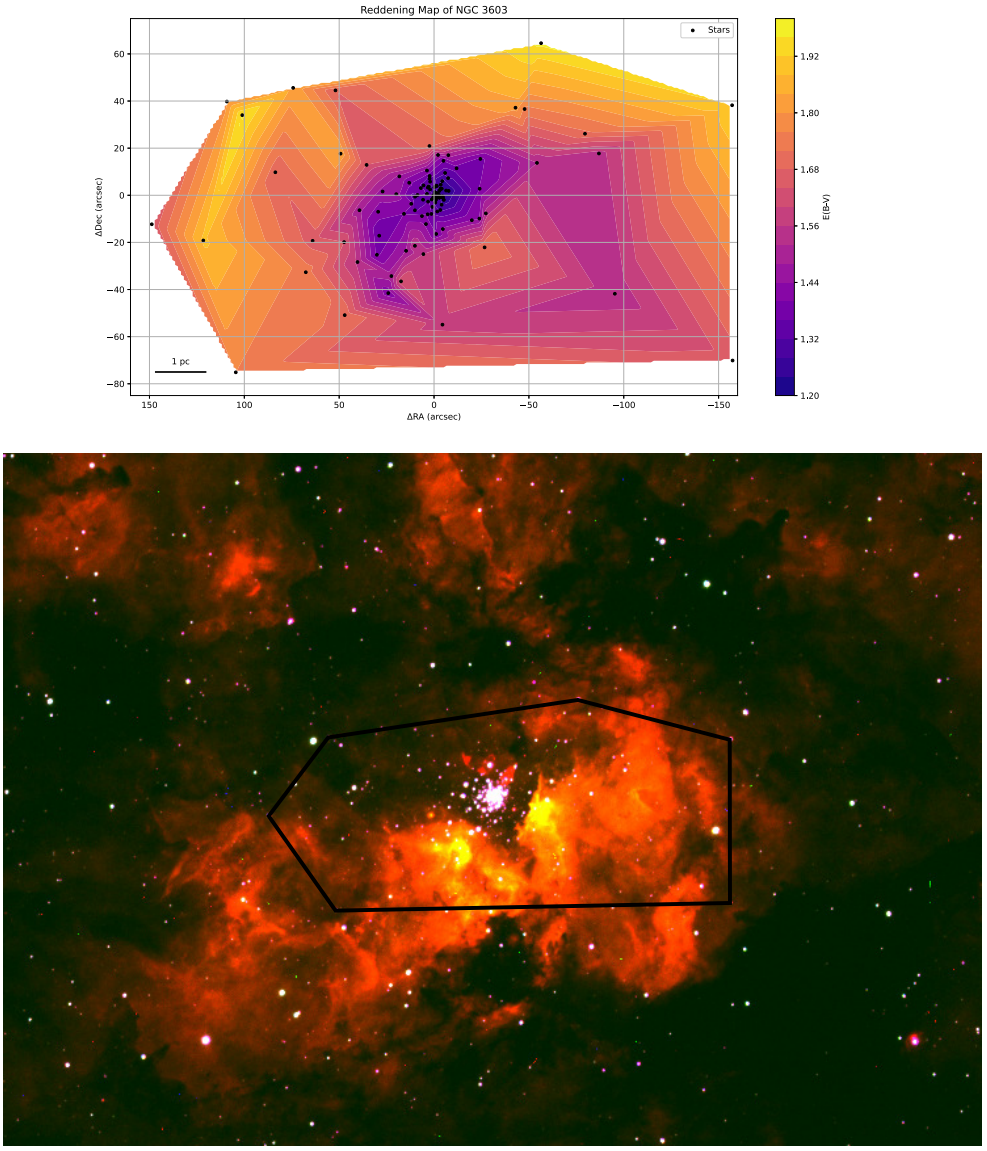

Figure 7. Reddening map of NGC 3603. Top: a smoothed contour map of the $E(B-V)$ values determined from the photometry of the stars spectroscopically classified as O type or early B. The axes show the distance in arcseconds from the center of the cluster, taken to be NGC 3603-A1. Note that the cluster center is located in a reddening "hole," presumably blown by the strong stellar winds of the numerous hot luminous stars present. Reddening increases toward the periphery of the region. Bottom: for comparison, we show a color rendition of the region. The image is the composite of a 300 s Hα on-band exposure (red), a 150 s Hα continuum exposure (blue), and a 300 s O III λ5007 on-band exposure (green). The data were taken by graduate student Kennedy Farrell and coauthor N.M. on UT 2025 January 6 on the Las Campanas 1 m Swope telescope at the end of the night during time assigned for an unrelated project.

as discussed above. The bolometric correction is just

$$\mathrm{BC} = -6.80 \log T_{\rm eff} + 27.58,$$

based on the study of F. Martins et al. (2005) as discussed above. The bolometric magnitude is

$$m_{\rm bol} = M_V + \mathrm{BC},$$

and the log of the bolometric luminosity relative to the Sun is computed as

$$\log L/L_\odot = (m_{\rm bol} - 4.74)/-2.5,$$

where 4.74 is the bolometric magnitude of the Sun.

5.1.1. Physical Parameters from Modeling

For NGC 3603 there are complications in addition to the usual complexities of modeling spectra. The main one is that, because of the high extinction, no UV data are available to establish the terminal velocities of the wind. Lacking this information, we computed our models adopting a value for the terminal velocity that is 2.6× the escape speed $v_{\rm esc}$ (R.-P. Kudritzki & J. Puls 2000), where the calculation of $v_{\rm esc}$ is based on the model's surface gravity g, radius (computed to match the absolute visual magnitude and effective temperature), and Eddington factor.

We modeled the optical spectra of the O stars using version 10 of FASTWIND (A. E. Santolaya-Rey et al. 1997). This version includes approximate line blanketing (A. Herrero et al. 2002; J. Puls et al. 2005). Although the FASTWIND code was eventually updated to provide a more exact treatment of the background elements (J. Puls 2017), this older version had been found to give adequate agreement with the "gold-standard" CMFGEN code (D. J. Hillier & D. L. Miller 1998; D. J. Hillier 2003, 2012) as shown by P. Massey et al. (2013).

Table 3
Modeling of NGC 3603 Stars

			Modeler 1 (CO)				Modeler 2 (MH)			
Star	Sp.Type	$T_{\rm eff}$(Adopted)	Teff	log g	$\dot{M}$[a]	$v \sin i$[b]	Teff	log g	$\dot{M}$[a]	$v \sin i$[b]
16	O3V((f))	47,750	47,500	4.0	3.0	180	48,000	3.9	1.5	180
38	O3.5V((f))	43,000	43,000	3.8	1.6	150	43,000	3.7	0.9	160
42	O3.5III	44,000	…	…	…	…	44,000	3.8	2.5	120
101	O6.5Vz	39,000	39,000	4.0	0.2	180	…	…	…	…
102	O8.5V/O9c	35,000	35,000	4.0	0.2	150	…	…	…	…
103	O3III((f*))	45,750	45,000	3.8	2.5	135	46,500	3.8	1.2	170
108	O4.5V	42,000	42,000	4.0	0.8	110	…	…	…	…
109	O8V	37,500	37,500	4.0	0.2	180	…	…	…	…
104	O3III((f*))	48,500	…	…	…	…	48,500	3.9	2.5	150
116	O3.5V((f))	45,000	45,000	4.0	0.2	150	…	…	…	…
117	O5.5V((f))z	40,000	40,000	4.0	0.4	330	…	…	…	…
120	O6V	40,750	40,500	4.0	0.2	110	41,000	4.0	0.2	130
124	O6V	37,500	37,500	3.8	0.2	130	…	…	…	…
125	O6V((f))	39,500	40,000	4.0	0.3	150	39,000	3.9	0.0	150
128	O9V	34,000	34,000	4.1	0.8	100	…	…	…	…
135	O8V	36,000	…	…	…	…	36,000	3.9	0.2	280
141	O8.5V	44,000	44,000	4.1	4.0	150	…	…	…	…
205	O2-O3III	43,500	43,500	3.9	1.6	120	52,000	4.0	2.0	120
210	O7V	37,000	…	…	…	…	37,000	3.8	0.2	230
214	O5.5V	39,000	…	…	…	…	39,000	3.7	0.2	115
215	O7V	37,000	37,000	4.0	0.7	200	…	…	…	…
216	O7.5V	36,000	36,000	4.0	0.1	260	…	…	…	…
218	O6.5V	37,000	35,500	3.4	0.2	130	38,500	4.0	0.2	120
219	O8V	37,000	37,000	4.0	0.2	300	…	…	…	…
220	O7.5V	36,000	36,000	4.0	0.5	400	…	…	…	…
222	O9.7V	34,000	…	…	…	…	34,000	4.0	0.0	120
227	B0.5V	31,000	31,000	4.1	0.5	250	…	…	…	…
305	O3.5V	44,250	42,000	3.8	0.5	200	46,500	4.0	0.4	170
308	O6V((f))	40,500	…	…	…	…	40,500	4.0	0.2	300
310	O5V	45,000	45,000	4.0	2.0	125	…	…	…	…
313	O6V	38,500	…	…	…	…	38,500	3.9	0.1	300
316	O3.5V	46,000	46,000	3.9	2.0	125	…	…	…	…
319	O3.5V	46,000	46,000	4.0	1.5	170	…	…	…	…
320	B0-B0.2V	30,000	30,000	4.1	0.1	160	…	…	…	…
334	O9.5V	33,500	33,500	3.8	0.2	160	…	…	…	…
Sh 17	O5.5III	39,750	40,000	3.8	0.8	135	39,500	3.9	1.7	140
Sh 19	O3V((f))	45,500	…	…	…	…	45,500	3.8	1.0	175
Sh 20	O9V	36,000	36,000	4.0	0.2	100	36,000	4.0	0.1	90
Sh 22	O3III(f)	48,500	…	…	…	…	48,500	4.0	5.0	200
Sh 23	OC 9.7Ia	29,000	…	…	…	…	29,000	3.1	2.2[c]	150
Sh 47	O3.5III(f)	47,000	…	…	…	…	47,000	4.1	2.5	210
Sh 48	O5.5V	40,000	…	…	…	…	40,000	3.7	0.7	240
Sh 50	O8.5III	36,000	…	…	…	…	36,000	3.9	0.2	170
Sh 52	O7V	36,500	…	…	…	…	36,500	4.0	0.0	200
Sh 57	O3III(f)	47,000	…	…	…	…	47,000	3.9	4.0	145
Sh 59	O8III	37,000	37,000	4.1	0.8	100	37,000	4.0	0.6	95
Sh 63	O3.5III((f))	44,500	…	…	…	…	44,500	3.7	0.8	170

Notes.
[a] Units of $10^{-6} M_{\odot}$ yr^{-1} computed with a filling factor f of 1.0. Actual mass-loss rates should be adjusted down by a factor of ~3 for standard clumping $f = 0.1$.
[b] Projected rotational velocity in units of km s^{-1}.
[c] Model computed with $\beta = 1.2$.

(This table is available in machine-readable form in the online article.)

The modeling was undertaken independently by two REU students, coauthors M.H. and C.O., with some stars in common to test consistency. The basic process is laid out in P. Massey et al. (2004). Adequate fits were all found with an adopted He/H number ratio of 0.1. In most cases, adopting the standard value $\beta = 0.8$ for the wind acceleration parameter was adequate; the one exception is noted in the table. The models were run without clumping, and thus the tabulated mass-loss rates should be corrected downward by a factor of $\sqrt{f}$, where f is the filling factor, usually taken to be 0.1. (In other words, the values should be decreased by roughly a factor of 3.) We note that the goal of this procedure was aimed at obtaining better effective temperatures than could be derived from just the spectral types, and not as a definitive analysis of their mass-loss rates or radii. This was particularly important for the earliest spectral types, as the classification scheme becomes

degenerate with effective temperatures as the He I lines weaken into the noise. (See discussion in P. Massey et al. 2004 and P. Massey et al. 2005.)

The results of this modeling effort are given in Table 3. We include the results from both modelers in order to show the excellent agreement despite the subjective procedure of judging the best fits by eye. The one exception is for the O2-3III star NGC 3603-205, where the lead author judged the results of the two fits.

5.1.2. Physical Parameters from Spectral Types

Not all of our spectra lent themselves to modeling; some spectra lacked the high signal-to-noise ratio that accurate modeling requires, and in other cases the wavelength coverage did not include Hα, crucial for determining the mass-loss rate $\dot{M}$. In particular, the O2-3I*f/WN5-6 "slash" stars required more sophisticated treatment than easily achieved with FASTWIND. For those stars, we adopted a value of 42,000 K, following the modeling of the (composite) spectrum of the NGC 3603-A1 binary (P. A. Crowther et al. 2010; see also P. Massey et al. 2025). For the other O-type stars that were not modeled but had spectral types, we relied on the theoretical calibration of spectral type and effective temperature by F. Martins et al. (2005) using CMFGEN models. Their results are in good agreement with the effective temperature scale found by P. Massey et al. (2005), derived by fitting LMC O-type stars with version 10 of FASTWIND.

For the B dwarfs, the temperature scale is much less well established. The most modern effort is that of C. Trundle et al. (2007), who applied a grid of TLUSTY to newly classified B stars as part of a large spectroscopic survey of massive stars. The values in their Table 10 only include early dwarfs for the Milky Way, and their B0 V temperature is actually hotter than what we adopt for an O9.5V star. To avoid this problem, we arrived at a compromise scale between their work and the scale given in Table 2 of W. Huang & D. R. Gies (2006). Those values trace to M. M. Hanson et al. (1997), which in turn got them from P. Massey et al. (1989), which was mostly based on P. J. Flower (1977). We propose that the problem with B dwarfs is twofold. First, unlike the O-type stars, the spectral classification criteria are somewhat poorly defined in terms of the relative strengths of Si II versus Si III versus Si IV line strengths. The problem is exacerbated by these lines being weaker at higher surface gravities (i.e., lower luminosities). Second, the modeling of these metal lines is certainly more complex than the case for the O stars, where the classification criteria are based primarily on the relative strengths of He I and He II: helium is a much simpler atom. The situation for our one B-type supergiant is considerably better, due to the CMFGEN modeling work of P. A. Crowther et al. (2006). For our B1Iab star Sh 25, we adopt an effective temperature of 21,000 K based on their work. (See also P. A. Crowther et al. 2008 and D. Weßmayer et al. 2023. The latter paper argues that Sh 25 is coincidentally a foreground star; we discuss this possibility further below in Section 5.3.)

We remind the reader that while an uncertainty in the temperature by itself is mostly parallel to the evolutionary tracks and thus does not affect our estimation of the mass, the luminosity is affected because of the dependence of the bolometric correction on the temperature, adding to its importance.

Table 4
Properties of NGC 3603 Stars with Spectra

Star	Sp.Type	$E(B-V)$	M_V	$\log T_{\rm eff}$	$\log L/L_\odot$	Type[a]
A1	O3If*/WN6	1.25	−7.28	4.623	6.35	3
B	O3If*/WN6	1.25	−7.13	4.623	6.29	2
C	O3If*/WN6	1.25	−6.56	4.623	6.06	2
Sh 25	B1Iab	1.69	−8.02	4.301	5.77	2
A2	O3V((f))	1.31	−6.19	4.649	5.99	2
Sh 18	O3.5If	1.56	−7.11	4.619	6.27	2
Sh 47	O3.5III(f)	1.48	−6.72	4.672	6.26	1
Sh 23	OC 9.7Ia	1.46	−6.62	4.462	5.65	1
301	O4Ifc	1.31	−5.95	4.610	5.78	2
42	O3.5III	1.30	−5.66	4.643	5.76	1
104	O3III((f*))	1.33	−5.77	4.686	5.92	1
302	O3.5V	1.26	−5.46	4.644	5.68	2
103	O3III((f*))	1.25	−5.35	4.660	5.68	1
A3	O3.5III(f)	1.32	−5.63	4.625	5.70	2
303	O3III	1.28	−5.37	4.633	5.61	2

Note.
[a] 1–$T_{\rm eff}$ determined by modeling (e.g., Table 3); 2–$T_{\rm eff}$ determined from spectral type; 3–$T_{\rm eff}$ determined by spectral type, but the system is binary.

(This table is available in its entirety in machine-readable form in the online article.)

5.1.3. The Final Parameters for Stars with Spectral Types

In Table 4 we list the physical properties we adopt for the member stars with spectroscopy. We indicate whether the parameters come from modeling or from the spectral types. For the binaries we adopted a temperature intermediate between the two components and computed the luminosity of the combined system, and we note these cases. (This decision is defended in Section 6.)

5.2. Stars without Spectroscopy

There are two problems for the stars without spectral types. The first of these is determining a membership probability for the stars without Gaia data. For the stars with spectroscopy, the Gaia data were somewhat superfluous, as a chance alignment of a rare O-type star with the cluster is negligible. However, for the stars without spectroscopy or Gaia data we must determine the probability of membership. There are 214 stars without spectroscopy but whose Gaia data suggest that they are likely members, usually with probabilities of 1.0. However, there are 143 stars without spectroscopy either that lack Gaia data or whose Gaia data are too poor to use (i.e., RUWE > 2.5). In order to address those, we utilized a "random forest" machine learning classifier on the stars' photometry, along with their radial distance from the cluster's center. We used the data of the known members and known nonmembers for training. The corresponding 3D probabilities as a function of location in the CMD are shown in the top left panel of Figure 8. As a reality check, we also ran the training data through the algorithm to see how clean the resulting separations are. The results are shown in the bottom panels of the figure.

This approach has the problem that there are few known members and nonmembers at faint magnitudes to provide guidance to the algorithm, and the classifier therefore relies heavily on the radial distance. However, there are few faint

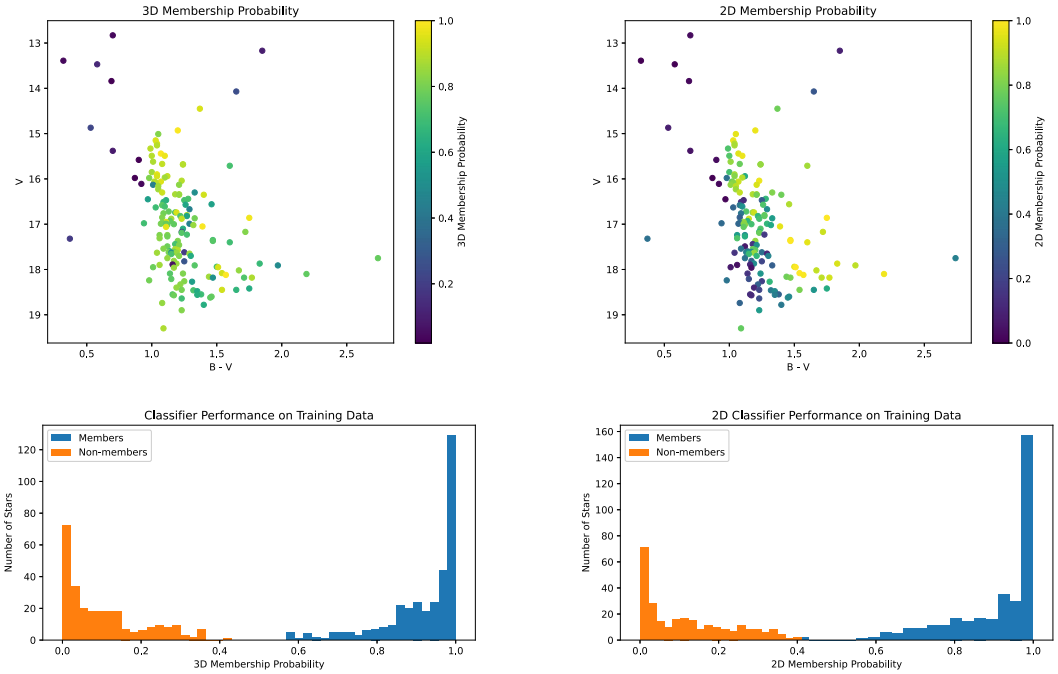

Figure 8. Membership probability for stars without spectroscopy. Top panels: for the stars without spectroscopy and without adequate Gaia data, we use a random forest machine learning classifier to assign probabilities of membership based on their location in the CMD. On the left we also include the star's radial distance from the center of the cluster in assigning probabilities. On the right we use only the magnitude and color information. The training data consist of the information on known members and known nonmembers. Bottom panels: results of applying the classifier on the training set itself as a reality check.

members or nonmembers known near the center of the cluster owing to the effects of crowding on the Gaia data and our need to focus our spectroscopy on the brighter members. Thus, there is a built-in bias toward assigning membership to stars with small radial distances. Applying the classifier using only the photometry (and not the radial distance) produces a much more pessimistic assessment of membership. We show the results of this 2D analysis on the right side of Figure 8. We retain both sets of probabilities in our analysis.

The second problem is how to assign physical properties to these stars. If we assume that the cluster is coeval, then the absolute visual magnitude M_V can be used to estimate the effective temperature. We use the reddening map in Figure 7 to approximate the $E(B-V)$ for all the stars without spectroscopy but whose Gaia data or location in the CMD suggest a probability of membership >50%. This allows us to compute the absolute visual magnitude M_V.

The vast majority of stars without spectroscopy (blue or black triangles in Figure 6) are fainter than the high-mass stars with the spectroscopy we have been discussing, and a reasonable assumption is that they are all dwarfs. For dwarfs we find an accurate relationship between effective temperature ($T_{\rm eff}$) and absolute visual magnitude (M_V):

$$T_{\rm eff} = 10605 - 3061.6 \times M_V + 516.53 \times M_V^2,$$

where we have extended the relationship between $T_{\rm eff}$ and M_V for O-type stars from F. Martins et al. (2005) to late B stars using the values given in Table 15.7 of A. N. Cox (2000). The scatter on that relationship is 450 K. Similarly, we use the BSTAR2006 models (T. Lanz & I. Hubeny 2007) with the CMFGEN models (F. Martins et al. 2005) to obtain an approximate relationship between the bolometric correction and absolute visual magnitude:

$$\mathrm{BC} = -0.06 + 0.60 \times M_V.$$

The scatter on that relationship is 0.04 mag.

We emphasize that these relations are approximate and rely heavily on the assumption that these stars with only photometry are located near the ZAMS. We list the derived physical parameters in Tables 5 and 6.

5.3. Comparison with Evolutionary Tracks

The goal of this project has been to count the number of stars as a function of mass, and for this we must compare the location of stars in the HRD to evolutionary tracks in order to assign masses. We show such a diagram in Figure 9, where we use the Geneva evolutionary models of S. Ekström et al. (2012) computed with rotation.

There is the expected plethora of massive stars, consistent with our spectroscopy. A few stars are found to the left of the ZAMS, presumably due to overestimating the effects of reddening, i.e., we expect that those stars have good temperatures (many were modeled) but are simply too low in the HRD. For the most part, the ages of stars are consistent with 1–3 Myr.

The most glaring exception is Sh 25. D. Weßmayer et al. (2023) argue on the basis of the star's luminosity that the star is in the foreground. Their modeling derives a $\log L/L_\odot$ of 5.48 based on a distance derived by an intriguing new method (D. Weßmayer et al. 2022), but one that requires an accurate assessment of the reddening (see Equation (3) in D. Weßmayer et al. 2022). We do not agree with this interpretation. First, the chances of a B1Iab just happening to be seen superposed on the NGC 3603 cluster are quite low. We back this up by noting that Sh 25 is the *only* B1 supergiant in our sample—they are rare. According to the Besançon model of the Milky Way, we

Table 5
Properties of NGC 3603 Stars without Spectroscopy but with Gaia Data

Star	V	$B-V$	Mem. Prob.	Reddening		M_V	$\log T_{\rm eff}$	$\log L/L_\odot$
				$E(B-V)$	S[a]			
2026	14.87	0.78	0.999	1.80	E	−5.95	4.673	5.73
2045	15.36	1.10	1.000	1.34	I	−3.48	4.440	4.15
2054	15.60	1.55	1.000	1.80	E	−5.22	4.610	5.26
2060	15.69	1.11	1.000	1.37	I	−3.28	4.418	4.02
2070	15.90	1.25	1.000	1.53	I	−3.78	4.471	4.34
2075	15.97	1.11	1.000	1.59	I	−3.93	4.486	4.44
1068	16.04	1.69	1.000	1.80	E	−4.78	4.569	4.98
2085	16.05	1.38	1.000	1.69	I	−4.31	4.524	4.68
2096	16.13	1.16	1.000	1.46	I	−3.22	4.412	3.98
2097	16.13	1.25	1.000	1.55	I	−3.64	4.456	4.25

Note.
[a] Source of reddening: I = interpolated; E = extrapolated.
(This table is available in its entirety in machine-readable form in the online article.)

Table 6
Properties of NGC 3603 Stars without Spectroscopy and without Gaia Data

Star	V	$B-V$	Mem. Prob.		Reddening		M_V	$\log T_{\rm eff}$	$\log L/L_\odot$
			3D	2D	$E(B-V)$	S[a]			
2020	14.45	1.37	0.94	0.78	1.40	I	−4.65	4.557	4.90
2027	14.93	1.20	0.99	0.97	1.39	I	−4.15	4.508	4.58
2029	15.01	1.05	0.82	0.96	1.44	I	−4.27	4.519	4.65
2034	15.15	1.03	0.94	0.97	1.33	I	−3.64	4.456	4.25
2037	15.22	1.04	0.94	0.89	1.30	I	−3.45	4.437	4.13
2040	15.26	1.04	0.89	0.87	1.37	I	−3.73	4.465	4.31
2044	15.33	0.99	0.90	0.72	1.26	I	−3.19	4.409	3.96
2048	15.44	1.07	0.99	0.95	1.31	I	−3.29	4.419	4.02
2050	15.49	1.00	0.89	0.73	1.25	I	−2.96	4.384	3.82
2051	15.49	1.10	0.97	0.97	1.36	I	−3.44	4.436	4.12

Note.
[a] Source of reddening: I = interpolated; E = extrapolated.
(This table is available in its entirety in machine-readable form in the online article.)

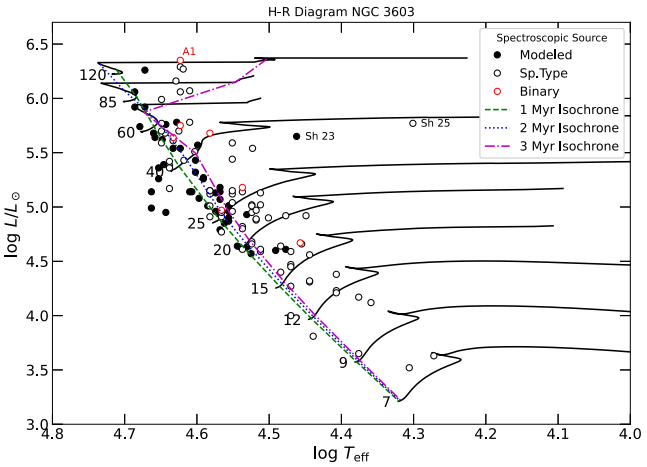

Figure 9. NGC 3603 HRD for stars with spectroscopy. The luminosities and effective temperatures determined with spectroscopy are plotted in this HRD. The data come from Table 4. The Geneva evolutionary tracks from S. Ekström et al. (2012) are shown by solid black lines, with their initial masses labeled near the beginning of the tracks. To simplify the figure, the tracks have been truncated. For the three highest-mass tracks ($60M_\odot$, $80M_\odot$, and $120M_\odot$) we stopped at the main-sequence turnoff (line 110 in the modes). For the others, we only show the tracks until the beginning of He burning (line 190 in the models). Isochrones have been computed using linear interpolation in the models.

expect to come across less than 10^{-2} OB supergiants per square degree at the Galactic latitude and longitude of NGC 3603. The area covered by our survey is 0.09 deg^2, so the superposition of a foreground B supergiant is indeed statistically unlikely.

We do agree with D. Weßmayer et al. (2023) that were Sh 25 a member it would be substantially older than the majority of the other OB stars. (They quote a value of 7 Myr, but that is based on the lower luminosity they derive.) However, this is not uncommon in otherwise coeval massive clusters. For instance, in their study of NGC 6611, L. A. Hillenbrand et al. (1993) find an age of 2 ± 1 Myr for the vast majority of stars and argue that, as far as the data could tell, most of the stars might have been formed on a particular Tuesday. Despite this, there is one "lower"-mass star ($30M_\odot$) with an age of about 6 Myr. They make the analogy to the popping of popcorn, with a few kernels going off before the great burst that pops most of the corn. Regardless of the possible facetiousness of the metaphor, the presence of an occasional older star in an otherwise coeval rich, massive cluster is not unprecedented. Besides NGC 6611, the reader is referred to the HRD of Cyg OB2 shown in P. Massey & A. B. Thompson (1991). R136 itself has such an example, the O8III star Mk 32. (See Table 1 and Figure 7 in P. Massey & D. A. Hunter 1998. Mk 32 is the

star at $\log T_{\rm eff} \sim 4.56$ and $M_{\rm bol} \sim 9.6$.) And here in NGC 3603 we find a second example: the OC 9.7Ia star Sh 23 is similarly a bit older. Of course, binary evolution could be invoked to explain these anomalous members. For the purposes of computing the slope of the IMF it is irrelevant whether we count Sh 25 as a member or not, but lacking compelling evidence to the contrary, we include it in our numbers below.

Near the bottom of the HRD we see a curious shift of the stars toward cooler temperatures. Are these stars misplaced? Without exception, all stars with spectroscopy and luminosities below $\log L/L_\odot = 4.5$ are the handful of early B-type stars we identified. As we previously noted, the effective temperature scale of B dwarfs is not as solidly determined as that of O-type stars, but can this fully explain their peculiar location? The two stars with the lowest assigned luminosities are 1093 (B2 III) with an adopted temperature of 20,200 K and 1112 (B3 V) with an assigned temperature of 18,700 K. To shift these stars close to the ZAMS would require their temperatures to be 20,800 K. This change is well within the uncertainties of both the spectral typing and the effective temperature scale once we get to the B stars. The fact that these are systematic further suggests that the problem is with the adopted scale.

We do not include the stars without spectroscopy in the plot, as the way we have extracted their physical properties from their photometry results in them simply paralleling the isochrones with a handful of stars between the $25M_\odot$ and $40M_\odot$ tracks until they become dominant at lower masses. We will demonstrate this numerically in the next section, where we consider the IMF slope.

6. The Slope of the IMF

E. E. Salpeter (1955) introduced the notion of an "original mass function."[15] Arguably, it was G. E. Miller & J. M. Scalo (1979) and B. M. Tinsley (1980) who put the study of SFRs and the IMF onto a modern footing. Using the notation of B. M. Tinsley (1980), the number of stars formed in the mass interval $(m, m+dm)$ in the time interval $(t, t+dt)$ is described as

$$\phi(m)\psi(t)\, dm\, dt,$$

where $\phi(m)$ is called the IMF and $\psi(t)$ is the SFR, the total mass of stars formed per unit time. $\phi(m)$ is normalized in such a way that $\int_0^\infty m\phi(m) \quad dm = 1$, and it is well described as a power law, with $\phi(m) \propto m^{-(1+x)}$. As B. M. Tinsley (1980) notes, x, $-x$, $(1 + x)$, and $-(1 + x)$ have all been called the slope of the IMF. We retain the terminology used in the introduction, where $\Gamma = -x$ is the slope. Following J. M. Scalo (1986), it is convenient to define the quantity $\xi(\log m)$ as the number of stars per mass bin normalized by the size of the bin expressed as the base-10 logarithm of the ratio of the upper and lower masses of the bin, as well as by the area expressed in units of kpc^2. Then, the slope of the mass function is simply $\Gamma = d \log \xi(\log m)/d \log m$. As a reminder, the E. E. Salpeter (1955) IMF slope has a nominal value of $\Gamma = -1.35$.

[15] Although E. E. Salpeter (1955) is often referenced only for the sake of the −1.35 value of the exponent of the mass function, this extraordinary paper did far more than that: using the luminosity function of main-sequence stars, the study successfully tested the hypothesis that stars evolve off the main sequence after burning ∼10% of their hydrogen mass, and it demonstrated that star formation has remained relatively constant in the solar neighborhood over the past five billion years. For more, see P. Kroupa & T. Jerabkova (2019).

Table 7
Number of Stars as a Function of Mass

Mass ($M_\odot$)	No. from Spectra	No. from Photometry			Total Number	
		Gaia	2D CMD	3D CMD	2D	3D
85–120	5	0	0	0	5	5
60–85	6	1	0	0	7	7
40–60	25	0	0	0	25	25
25–40	38	3	0.9	0.7	41.9	41.7
20–25	22	4.4	0.8	0.9	27.2	27.3
15–20	18	16.9	5.5	5.2	40.4	40.1
12–15	5	25.2	7.1	5.9	37.2	36.1
9–12	5	48.4	11.3	11.6	64.6	64.9
7–9	2	50.9	23.8	26.0	76.7	78.9

Of course, what one actually measures is the present-day mass function (PDMF). The connection between the PDMF and IMF depends on the star-forming history. When talking about an extended region containing many star-forming regions, one might assume a continuous SFR and adjust the counts by the relative main-sequence lifetimes as a function of mass; at the other extreme, a single cluster or OB association may be considered to be coeval (or at least "mostly" coeval) and the slopes of the IMF and PDMF the same, but note that the uppermost part of the PDMF may have been depleted relative to the IMF by stellar evolution, or the slope steepened by ejection of lower-mass stars (see, e.g., M. Marks et al. 2012 and S. Banerjee & P. Kroupa 2012). Here we will assume that the PDMF and the IMF are the same, but keep in mind these caveats.

To derive the mass function slope of NGC 3603, we begin by counting the number of stars between successive massive tracks. We give these numbers in Table 7, denoting which stars had been placed by spectroscopy and which by photometry. The stars that were placed on the basis of spectroscopy are certain members given their early types, but for the stars with only photometry we count "fractional stars" based on their probability of membership, as determined in the previous sections. In Figure 10 we show the number of stars in each mass bin that have been placed by spectroscopy and photometry.

Using the data from Table 7, we calculate the values of $\log \xi$, and we show these in Table 8. We take the surface area to be 1.5×10^{-4} kpc^2, corresponding to our survey area. The uncertainties listed are simply the stochastical $\sqrt{N}$ values to allow for the effects of small number statistics.

In Figure 11 we show the run of $\log \xi$ with the log of the mass. We continue this down to the $7M_\odot$ track.[16] We see that values through the $60M_\odot$ track are well represented by a straight line. The two highest-mass bins, $60M_\odot$–$85M_\odot$ and $85M_\odot$–$120M_\odot$, are depleted relative to the other data. Fitting all the points, weighting the data to take the stochastical uncertainties into account, yields a mass function slope $\Gamma = -0.97 \pm 0.09$. Ignoring the two higher-mass points results in a fit with $\Gamma = -0.87 \pm 0.10$. The same result is

[16] As mentioned earlier, our photometry is relatively complete to $V = 18.0$–18.5 and $B = 19.0$–19.5. With $E(B - V) = 1.2$–1.8, we find that in the worse case the photometry extends down to an $M_V = -2.8$, or $\log L/L_\odot = 3.3$. As we see by comparison with Figure 9, this roughly corresponds to $7M_\odot$.

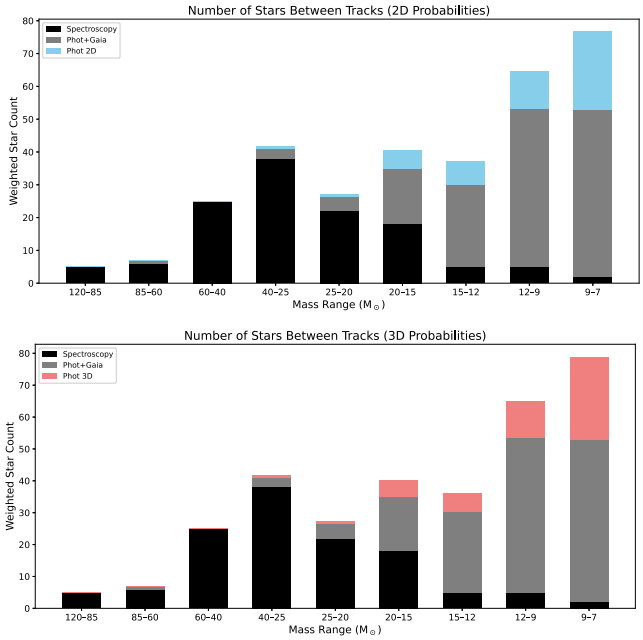

Figure 10. The contribution of spectroscopy and photometry to the number of stars in each mass bin. The black bars denote the number of stars in each mass bin that were placed by means of spectroscopy, either by modeling or from the spectral types. The gray boxes denote the stars without spectroscopy but with Gaia data indicating a membership probability. The colored bars (blue for 2D and red for 3D) denote the contribution from stars whose membership probabilities were determined on the basis of location in the CMD.

Table 8
Mass Function

Mass m ($M_\odot$)	$\overline{\log m}$ ($M_\odot$)	$\xi(\log m)$ 2D	$\xi(\log m)$ 3D
85–120	2.004	$5.35^{+0.16}_{-0.26}$	$5.35^{+0.16}_{-0.26}$
60– 85	1.854	$5.49^{+0.14}_{-0.21}$	$5.49^{+0.14}_{-0.21}$
40–60	1.690	$5.98^{+0.08}_{-0.10}$	$5.98^{+0.08}_{-0.10}$
25–40	1.500	$6.14^{+0.06}_{-0.07}$	$6.13^{+0.06}_{-0.07}$
20–25	1.349	$6.27^{+0.08}_{-0.09}$	$6.27^{+0.08}_{-0.09}$
15–20	1.239	$6.33^{+0.06}_{-0.07}$	$6.33^{+0.06}_{-0.07}$
12–15	1.128	$6.41^{+0.07}_{-0.08}$	$6.40^{+0.07}_{-0.08}$
9–12	1.017	$6.54^{+0.05}_{-0.06}$	$6.54^{+0.05}_{-0.06}$
7–9	0.900	$6.67^{+0.05}_{-0.05}$	$6.68^{+0.05}_{-0.05}$

obtained whether we use the 2D or 3D memberships from the CMD for the stars without spectroscopy and without Gaia data.

Furthermore, we see from Figure 10 that the stars whose placement is determined by photometry do not become dominant until the $12M_\odot$–$15M_\odot$ bin ($\overline{\log m} = 1.128$). Yet there is no discontinuity present. Indeed, if we had restricted our calculation only to the three points ($20M_\odot$–$25M_\odot$, $25M_\odot$–$40M_\odot$, $40M_\odot$–$60M_\odot$), we would get essentially the same slope, -0.85 rather than -0.87.

Throughout the 1990s and early 2000s the lead author and various collaborators measured the IMF slope in OB associations in the Magellanic Clouds and Milky Way. Examples of well-known regions include NGC 346 in the SMC (P. Massey et al. 1989), R136 (P. Massey & D. A. Hunter 1998), NGC 6611 (L. A. Hillenbrand et al. 1993), Cyg OB2 (P. Massey & J. Johnson 1993) and h/Chi Per in the Milky Way (C. L. Slesnick et al. 2002). The results of these studies are summarized in Table 1 of P. Massey (2011). For the 25 OB associations and clusters with well-defined IMFs, the values of Γ ranged from -0.7 ± 0.2 to -2.1 ± 0.6. The median value is -1.3, and the average weighted value is -1.2 with an rms (1σ variation) of 0.3. No correlation was found with metallicity or stellar density. All 25 of the regions, as well as our study here, were done in the same manner, including simply treating binaries as if they were single stars. Of course, to derive the *actual* IMF, these values must be corrected for the influence of unresolved binaries, as emphasized by P. Kroupa (2007). Lower-mass stars may have been ejected from the cluster core, steepening the IMF, but hopefully we have avoided this by analyzing a region much larger than the central cluster. Hence, while none of these values are completely right, they have all been carried out in an identical manner, and thus comparisons are valid.

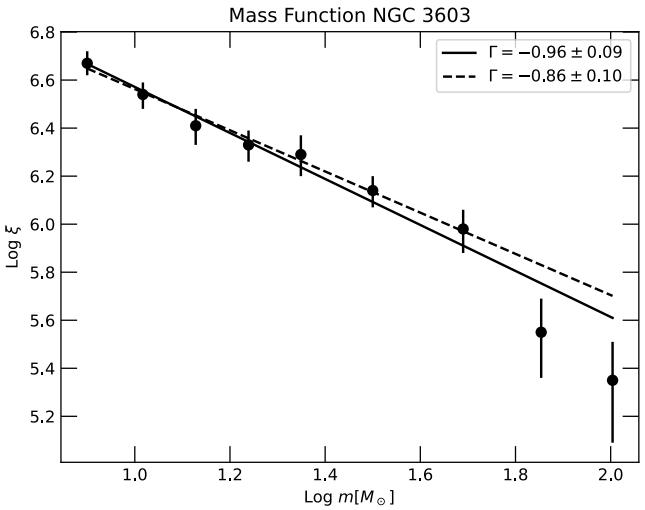

Figure 11. The mass function of NGC 3603. The data from the 2D ξ values are plotted; the 3D values are indistinguishable. The error bars denote the expected $\sqrt{N}$ stochastical variations. The solid line shows the linear fit for all the data; the dashed line shows the fit ignoring the two highest-mass bins.

Thus, with the result here we feel we can definitively answer the question posed in the title of the paper: no, the mass function of NGC 3603 is not top-heavy. The slope determined from stars in the range of $7M_\odot$–$60M_\odot$, $\Gamma = -0.9 \pm 0.1$, is no different than that of other well-studied regions analyzed in the same manner.

7. Summary and Discussion

Ground-based and ACS imaging provided photometry of 764 stars. Most of these have Gaia astrometry that allows us to identify probability of membership in NGC 3603. Using spectra collected over many years at both Magellan and HST, we have characterized the physical properties of 129 of the brightest members, including 30 whose properties were determined by modeling. For the remaining stars for which there are no spectroscopy, we established membership probabilities either from Gaia data or from their location in the CMD. The resulting HRD shows a very young (1–3 Myr) rich population of massive stars up to $120+M_\odot$. A few stars (e.g., Sh 25 and Sh 24) appear to be a few million years older, suggesting that the cluster formation was not strictly coeval. This is similar to what we observe in some other clusters, for

instance, NGC 6611 (L. A. Hillenbrand et al. 1993). We have analyzed the mass function of this cluster using the same technique previously applied to 25 SMC, LMC, and Galactic OB associations (P. Massey 2011 and references therein), finding that there is nothing unusual in its slope.

Rather than being top-heavy, if anything there are stars missing in the $60M_{\odot}$–$120M_{\odot}$ range. Given the slope and intercept of our fit without these points, we calculate that there should be 25.9 $\pm$ 13.7 stars in that group. We count only 11 (Table 7), 10 of which were placed by means of spectroscopy and one by photometry. In the case of somewhat older clusters, such as h and χ Per, the uppermost mass bin contains fewer stars than what we would expect based on extrapolation from other bins. This is easily explained by stellar evolution depleting the higher-mass bin. However, here in NGC 3603 we would require something like 14 high-mass stars to have gone through core collapse. While there is clearly a gas-free bubble surrounding the central cluster (Figure 7), we expect that 14 supernovae going off in the past few Myr in this region would have had a significantly more disruptive effect. While it is true that some massive stars may undergo core collapse without the usual fireworks, traditionally this was expected predominantly for the highest-mass stars at subsolar metallicity (e.g., A. Heger et al. 2003). In addition, recent work has suggested that the situation is more complex, with the detailed core structure and the time of core collapse leading to nonmonotonic "islands of explodability." For example, T. Sukhbold et al. (2016) predict that stars with initial masses near $25M_{\odot}$ and $30M_{\odot}$ may undergo direct collapse, whereas several higher-mass models may yield successful explosions (see their Figure 13). In addition, observational searches for failed supernovae in nearby galaxies have thus far yielded only a few candidates, which are predominantly yellow or red supergiants at intermediate ($\sim 25M_{\odot}$) masses (see, e.g., J. R. Gerke et al. 2015; T. M. Reynolds et al. 2015). Regardless, 14 is a lot of massive stars to have gone quietly.

This suggests that the formation of the highest-mass stars may actually have been slightly discouraged in NGC 3603. This is not something we see in the even richer region R136 on the LMC (P. Massey & D. A. Hunter 1998; J. M. Bestenlehner et al. 2020), but the metallicity of NGC 3603 is presumably 2$\times$ higher. What, then, could lead to such a suppression? The question of what limits the ultimate mass of a star remains unanswered. R. B. Larson & S. Starrfield (1971) expected that accretion would be stopped by the effects of radiative heating, radiation pressure, and/or ionization. They argued that the latter would be the dominant effect: as an H II region forms in the protostellar material, the temperature rises by several orders of magnitude, and the resulting pressure stops the infall. Later, radiation pressure was thought to be the limiting factor (e.g., M. G. Wolfire & J. P. Cassinelli 1987), but that, too, has been discounted: self-shielding is thought to allow the pressure to be relieved through thin bubbles (M. R. Krumholz et al. 2009) or bipolar outflows (R. Banerjee & R. E. Pudritz 2007). Recent papers suggest that radiatively driven winds (J. S. Vink 2018) or UV line-driven disk ablation (N. D. Kee & R. Kuiper 2019, 2024) may provide the limiting factors. Such mechanisms are metallicity dependent. Very high masses ($200M_{\odot}$–$300M_{\odot}$) have been attributed to stars like R136a1 in the LMC based on atmospheric and evolutionary modeling (see, e.g., P. A. Crowther et al. 2010; J. M. Bestenlehner et al. 2020). However, even if this is correct, it may be that in the higher-metallicity environment of the Milky Way (i.e., NGC 3603) the limit may be lower and may begin to depress star formation at the upper end of the IMF. Why we do not see this same effect in other Galactic clusters may simply be the richness of NGC 3603: none of the previously analyzed regions are as strongly populated with such high-mass stars. Perhaps the "upper mass limit" is not a hard cutoff, but rather lowers the star formation probability down a few notches.

The "observed" upper limit to the mass of a star is also poorly known. There are many stars whose masses have been inferred to be well above $100M_{\odot}$; these have become known as very massive stars (VMSs). The most well-known of these is the central star in the R136 cluster, R136a1, for which P. A. Crowther et al. (2010) derived a mass of $200M_{\odot}$–$300M_{\odot}$. In fact, Z. Keszthelyi et al. (2025) suggest that the initial mass of R136a1 was $\sim 350M_{\odot}$ and that two other stars in the core, R136a2 and R136a3, had initial masses $>500M_{\odot}$![17] Based on evolutionary tracks and atmosphere modeling of their luminosities, J. M. Bestenlehner et al. (2020) identified seven VMSs in the R136 cluster. In the Milky Way, the luminosities of such stars have sometimes been overestimated owing to undetected multiplicity. For instance, N. R. Walborn et al. (2002) estimate the mass of Pismis 24-1 to be $200M_{\odot}$–$300M_{\odot}$, but the star was subsequently identified to be a previously unrecognized triple system by J. Maíz Apellániz et al. (2007). Still, given the preponderance of VMSs and the claim of large binary fractions for massive stars (e.g., H. Sana et al. 2012), it is perhaps surprising that the highest masses reliably measured through binary motion remain in the $90M_{\odot}$–$100M_{\odot}$ range (see Table 5 in P. Massey et al. 2025). Finally, we recall that J. J. Eldridge (2012) emphasized that binarity can affect any "observed" upper mass limit, given that mass transfer can produce stars with higher masses than could form by more pristine star formation processes.

Regardless of why the two high-mass bins are depressed relative to those of lower mass, our data suggest that the IMF of NGC 3603 is not top-heavy as some have expected. Whether there are actual variations in the slope of the IMF will doubtless remain a lively topic of debate for the foreseeable future, but we note that both R136 and NGC 3603 provide examples of rather extreme environments where there is no evidence of such variations.[18]

Acknowledgments

Lowell Observatory sits at the base of mountains sacred to tribes throughout the region. We honor their past, present, and future generations, who have lived here for millennia and will forever call this place home.

The observations presented here were obtained over years at Las Campanas Observatory, and we are grateful to the excellent technical and logistical support we have always received there. We also acknowledge long-term support by both the Carnegie and Arizona Time Allocation Committees. Obtaining the crucial IMACS multislit data was made possible

[17] Such numbers now approach the $1000M_{\odot}$ mass once attributed to R136a (B. D. Savage et al. 1983) before adaptive optics and HST showed that it was a tight cluster.

[18] A colleague of ours recently quipped that there is a 50 Mpc "rule" about the IMF slope: at any distance where it is currently impossible to verify the IMF via resolved stellar populations, studies will conclude that the IMF *must* vary. Studies of regions at distances small enough to actually do the measurements will always conclude that the IMF is universal. Of course, there are exceptions to this adage, most notably the recent study by S. K. Li et al. (2025).

with help from Dr. Carlos Contreras, and the installation and use of the COSMOS3 reduction software benefited from email exchanges with Drs. Gus Oemler and Daniel Kelson.

Partial support for this work was provided by the National Science Foundation (NSF) through AST-2307594 awarded to P.M. In addition, support for K.F.N. was provided by NASA through the NASA Hubble Fellowship grant HST-HF2-51516 awarded by the Space Telescope Science Institute, which is operated by the Association of Universities for Research in Astronomy, Inc., for NASA, under contract NAS5-26555. Additional support for the analysis was provided by NASA through grants GO-6299.001 and AR-17553.001. Support for the REU students was provided by the NSF through site awards 1004107, 1852478, and 1950901.

We are grateful to many of our colleagues for help and advice throughout this work. Dr. Joachim Puls provided us with his FASTWIND code many years ago. Our thoughts and discussion of the IMF benefited from conversations and correspondence with Drs. Deidre Hunter, Gerhardt Meurer, Jacqueline Monkiewicz, Joel Parker, and Sumner Starrfield. We are grateful to a quasi-anonymous referee for useful comments that improved the presentation.

Some assistance in Python programming (including the covariance probability assignment from Gaia data, the top panel of Figure 7, and the random forest machine learning classifier) was provided by ChatGPT-4 (OpenAI et al. 2023).

This work has made use of data from the European Space Agency (ESA) mission Gaia (https://www.cosmos.esa.int/gaia), processed by the Gaia Data Processing and Analysis Consortium (DPAC, https://www.cosmos.esa.int/web/gaia/dpac/consortium). Funding for the DPAC has been provided by national institutions, in particular the institutions participating in the Gaia Multilateral Agreement.

Facilities: HST (STIS, ACS), Gaia, Magellan: Clay (MIKE, MagE), Magellan: Baade (MagE, IMACS), Swope (SITe No. 3 imaging camera, E2V CCD231-84 imaging camera), CTIO 1.0 m (Y4KCam), CTIO 1.3 m (ANDICAM).

ORCID iDs

Philip Massey https://orcid.org/0000-0001-6563-7828
Nidia I. Morrell https://orcid.org/0000-0003-2535-3091
Kathryn F. Neugent https://orcid.org/0000-0002-5787-138X
Maria R. Drout https://orcid.org/0000-0001-7081-0082

References

Banerjee, S., & Kroupa, P. 2012, A&A, 547, A23
Banerjee, R., & Pudritz, R. E. 2007, ApJ, 660, 479
Bernstein, R., Shectman, S. A., Gunnels, S. M., Mochnacki, S., & Athey, A. E. 2003, Proc. SPIE, 4841, 1694
Bestenlehner, J. M., Crowther, P. A., Caballero-Nieves, S. M., et al. 2020, MNRAS, 499, 1918
Cannon, A. J., & Mayall, M. W. 1949, AnHar, 112, 1
Conti, P. S. 1973, ApJ, 179, 181
Conti, P. S., & Bohannan, B. 1989, in Astrophysics and Space Science Library, Vol. 157, IAU Colloq. 113: Physics of Luminous Blue Variables, ed. K. Davidson, A. F. J. Moffat, & H. J. G. L. M. Lamers (Dordrecht: Springer), 297
Cox, A. N. 2000, Allen's Astrophysical Quantities (New York: Springer)
Crowther, P. A., & Dessart, L. 1998, MNRAS, 296, 622
Crowther, P. A., Hirschi, R., Walborn, N. R., & Yusof, N. 2012, in ASP Conf. Ser. 465, Proc. of a Scientific Meeting in Honor of Anthony F. J. Moffat (San Francisco, CA: ASP), 196
Crowther, P. A., Lennon, D. J., & Walborn, N. R. 2006, A&A, 446, 279
Crowther, P. A., Lennon, D. J., Walborn, N. R., & Smartt, S. J. 2008, in ASP Conf. Ser. 388, Mass Loss from Stars and the Evolution of Stellar Clusters, ed. A. de Koter, L. J. Smith, & L. B. F. M. Waters (San Francisco, CA: ASP), 109
Crowther, P. A., Schnurr, O., Hirschi, R., et al. 2010, MNRAS, 408, 731
de Koter, A., Heap, S. R., & Hubeny, I. 1997, ApJ, 477, 792
Dressler, A., Bigelow, B., Hare, T., et al. 2011, PASP, 123, 288
Drissen, L., Moffat, A. F. J., Walborn, N. R., & Shara, M. M. 1995, AJ, 110, 2235
Ekström, S., Georgy, C., Eggenberger, P., et al. 2012, A&A, 537, A146
Eldridge, J. J. 2012, MNRAS, 422, 794
Elmegreen, B. G. 2005, in Astrophysics & Space Science Library, Vol. 329, Starbursts: From 30 Doradus to Lyman Break Galaxies, ed. R. de Grijs & R. M. González Delgado (Dordrecht: Springer), 57
Elmegreen, B. G. 2011, ApJ, 731, 61
Fitzgerald, M. P. 1970, A&A, 4, 234
Fitzpatrick, M., Placco, V., Bolton, A., et al. 2024, arXiv:2401.01982
Flower, P. J. 1977, A&A, 54, 31
Gaia Collaboration 2022, yCat, 1355, 0
Gaia Collaboration, Prusti, T., de Bruijne, J. H. J., et al. 2016, A&A, 595, A1
Gaia Collaboration, Vallenari, A., Brown, A. G. A., et al. 2023, A&A, 674, A1
Gerke, J. R., Kochanek, C. S., & Stanek, K. Z. 2015, MNRAS, 450, 3289
Gräfener, G., Vink, J. S., de Koter, A., & Langer, N. 2011, A&A, 535, A56
Gray, R. O., & Corbally, C. J. 2009, Stellar Spectral Classification (Princeton, NJ: Princeton Univ. Press)
Hanson, M. M., Howarth, I. D., & Conti, P. S. 1997, ApJ, 489, 698
Harayama, Y., Eisenhauer, F., & Martins, F. 2008, ApJ, 675, 1319
Heger, A., Fryer, C. L., Woosley, S. E., Langer, N., & Hartmann, D. H. 2003, ApJ, 591, 288
Herrero, A., Puls, J., & Najarro, F. 2002, A&A, 396, 949
Hillenbrand, L. A., Massey, P., Strom, S. E., & Merrill, K. M. 1993, AJ, 106, 1906
Hillier, D. J. 2003, in IAU Symp. 212, A Massive Star Odyssey: From Main Sequence to Supernova, ed. K. van der Hucht, A. Herrero, & C. Esteban (Cambridge: Cambridge Univ. Press), 70
Hillier, D. J., & Miller, D. L. 1998, ApJ, 496, 407
Hillier, D. J., Richards, M. T., & Hubeny, I. 2012, in IAU Symp. 282, From Interacting Binaries to Exoplanets: Essential Modeling Tools (Cambridge: Cambridge Univ. Press), 229
Hofmann, K. H., & Weigelt, G. 1986, A&A, 167, L15
Huang, W., & Gies, D. R. 2006, ApJ, 648, 580
Huchra, J. P. 1977, ApJ, 217, 928
Kee, N. D., & Kuiper, R. 2019, MNRAS, 483, 4893
Kee, N. D., & Kuiper, R. 2024, in IAU Symp. 361, Massive Stars Near and Far, ed. J. Mackey, J. S. Vink, & N. St-Louis (Cambridge: Cambridge Univ. Press), 550
Keszthelyi, Z., Brands, S. A., de Koter, A., Langer, N., & Puls, J. 2025, A&A, 700, A186
Kroupa, P. 2001, MNRAS, 322, 231
Kroupa, P. 2002, in ASP Conf. Ser. 285, Modes of Star Formation and the Origin of Field Populations, ed. E. K. Grebel & W. Brandner (San Francisco, CA: ASP), 86
Kroupa, P. 2007, in IAU Symp. 241, Stellar Populations as Building Blocks of Galaxies, ed. A. Vazdekis & R. Peletier (Cambridge: Cambridge Univ. Press), 109
Kroupa, P., & Jerabkova, T. 2019, NatAs, 3, 482
Krumholz, M. R., Klein, R. I., McKee, C. F., Offner, S. S. R., & Cunningham, A. J. 2009, Sci, 323, 754
Kudritzki, R.-P., & Puls, J. 2000, ARA&A, 38, 613
Lang, D., Hogg, D. W., Mierle, K., Blanton, M., & Roweis, S. 2010, AJ, 139, 1782
Lanz, T., & Hubeny, I. 2007, ApJS, 169, 83
Larson, R. B., & Starrfield, S. 1971, A&A, 13, 190
Leitherer, C. 2011, in APS Conf. Ser. 440, UP2010: Have Observations Revealed a Variable Upper End of the Initial Mass Function?, ed. M. Treyer et al. (San Francisco, CA: ASP), 309
Li, S. K., Diego, J. M., Meena, A. K., et al. 2025, ApJ, 988, 178
Lindegren, L., Klioner, S. A., Hernández, J., et al. 2021, A&A, 649, A2
Maíz Apellániz, J., Walborn, N. R., Morrell, N. I., Niemela, V. S., & Nelan, E. P. 2007, ApJ, 660, 1480
Marks, M., Kroupa, P., Dabringhausen, J., & Pawlowski, M. S. 2012, MNRAS, 422, 2246
Marshall, J. L., Burles, S., Thompson, I. B., et al. 2008, Proc. SPIE, 7014, 701454
Martins, F., & Plez, B. 2006, A&A, 457, 637

Martins, F., Schaerer, D., & Hillier, D. J. 2005, A&A, 436, 1049
Massey, P. 1998, in ASP Conf. Ser. Vol. 142, The Stellar Initial Mass Function (38th Herstmonceux Conf.), ed. G. Gilmore & D. Howell (San Francisco: ASP), 17
Massey, P. 2011, in ASP Conf. Ser. 440, UP2010: Have Observations Revealed a Variable Upper End of the Initial Mass Function?, ed. M. Treyer et al. (San Francisco: ASP), 29
Massey, P., Bodansky, S., Penny, L. R., & Neugent, K. F. 2025, ApJ, 990, 52
Massey, P., Bresolin, F., Kudritzki, R. P., Puls, J., & Pauldrach, A. W. A. 2004, ApJ, 608, 1001
Massey, P., & Hanson, M. M. 2013, in Planets, Stars and Stellar Systems. Vol. 2: Astronomical Techniques, Software and Data, ed. T. D. Oswalt & H. E. Bond (Dordrecht: Springer), 35
Massey, P., & Hunter, D. A. 1998, ApJ, 493, 180
Massey, P., & Johnson, J. 1993, AJ, 105, 980
Massey, P., Morrell, N. I., Neugent, K. F., et al. 2012, ApJ, 748, 96
Massey, P., Neugent, K. F., Hillier, D. J., & Puls, J. 2013, ApJ, 768, 6
Massey, P., Parker, J. W., & Garmany, C. D. 1989, AJ, 98, 1305
Massey, P., Puls, J., Pauldrach, A. W. A., et al. 2005, ApJ, 627, 477
Massey, P., & Thompson, A. B. 1991, AJ, 101, 1408
Melena, N. W., Massey, P., Morrell, N. I., & Zangari, A. M. 2008, AJ, 135, 878
Melnick, J., Tapia, M., & Terlevich, R. 1989, A&A, 213, 89
Meurer, G. R., Wong, O. I., Kim, J. H., et al. 2009, ApJ, 695, 765
Miller, G. E., & Scalo, J. M. 1979, ApJS, 41, 513
Moffat, A. F. J., Drissen, L., & Shara, M. M. 1994, ApJ, 436, 183
Moffat, A. F. J., & Niemela, V. S. 1984, ApJ, 284, 631
Mowlavi, N., Holl, B., Lecoeur-Taïbi, I., et al. 2023, A&A, 674, A16
OpenAI, Achiam, J., Adler, S., et al. 2023, arXiv:2303.08774
Pandey, A. K., Ogura, K., & Sekiguchi, K. 2000, PASJ, 52, 847
Pang, X., Pasquali, A., & Grebel, E. K. 2016, AJ, 151, 23
Puls, J. 2017, in IAU Symp. 329, The Lives and Death-Throes of Massive Stars, ed. J. J. Eldridge et al. (Cambridge: Cambridge Univ. Press), 435
Puls, J., Urbaneja, M. A., Venero, R., et al. 2005, A&A, 435, 669
Reynolds, T. M., Fraser, M., & Gilmore, G. 2015, MNRAS, 453, 2885
Rickman, E., & Brown, J. 2024, Hubble Space Telescope User Documentation, STIS Instrument Handbook, Version 24.0 (Baltimore, MD: STScI)
Rieke, G. H., Lebofsky, M. J., Thompson, R. I., Low, F. J., & Tokunaga, A. T. 1980, ApJ, 238, 24
Rieke, G. H., Loken, K., Rieke, M. J., & Tamblyn, P. 1993, ApJ, 412, 99
Rogers, C., Brandl, B., & De Marchi, G. 2024, A&A, 688, A111
Roman-Lopes, A. 2012, MNRAS, 427, L65
Roman-Lopes, A. 2013a, MNRAS, 433, 712
Roman-Lopes, A. 2013b, MNRAS, 435, L73
Salpeter, E. E. 1955, ApJ, 121, 161
Sana, H., de Mink, S. E., de Koter, A., et al. 2012, Sci, 337, 444
Santolaya-Rey, A. E., Puls, J., & Herrero, A. 1997, A&A, 323, 488
Savage, B. D., Fitzpatrick, E. L., Cassinelli, J. P., & Ebbets, D. C. 1983, ApJ, 273, 597
Scalo, J. 1990, in Astrophysics and Space Science Library, Vol. 160, Windows on Galaxies, ed. G. Fabbiano, J. S. Gallagher, & A. Renzini (Dordrecht: Kluwer), 125
Scalo, J. M. 1986, FCPh, 11, 1
Schneider, F. R. N., Sana, H., Evans, C. J., et al. 2018, Sci, 359, 69
Schnurr, O., Moffat, A. F. J., St-Louis, N., Morrell, N. I., & Guerrero, M. A. 2008, MNRAS, 389, 806
Shadmehri, M., & Elmegreen, B. G. 2011, MNRAS, 410, 788
Sher, D. 1965, MNRAS, 129, 237
Slesnick, C. L., Hillenbrand, L. A., & Massey, P. 2002, ApJ, 576, 880
Sota, A., Maíz Apellániz, J., Walborn, N. R., et al. 2011, ApJS, 193, 24
Stetson, P. B. 1987, PASP, 99, 191
Sukhbold, T., Ertl, T., Woosley, S. E., Brown, J. M., & Janka, H. T. 2016, ApJ, 821, 38
Tinsley, B. M. 1980, FCPh, 5, 287
Tody, D. 1986, Proc. SPIE, 627, 733
Tody, D. 1993, in ASP Conf. Ser. 52, Astronomical Data Analysis Software and Systems II, ed. R. J. Hanisch, R. J. V. Brissenden, & J. Barnes (San Francisco, CA: ASP), 173
Trundle, C., Dufton, P. L., Hunter, I., et al. 2007, A&A, 471, 625
van den Bergh, S. 1978, A&A, 63, 275
van den Bos, W. H. 1928, BAN, 4, 261
Vink, J. S. 2018, A&A, 615, A119
Walborn, N. R. 1982, ApJL, 254, L15
Walborn, N. R., & Fitzpatrick, E. L. 1990, PASP, 102, 379
Walborn, N. R., Howarth, I. D., Lennon, D. J., et al. 2002, AJ, 123, 2754
Walborn, N. R., Sana, H., Simón-Díaz, S., et al. 2014, A&A, 564, A40
Weßmayer, D., Przybilla, N., & Butler, K. 2022, A&A, 668, A92
Weßmayer, D., Przybilla, N., Ebenbichler, A., Aschenbrenner, P., & Butler, K. 2023, A&A, 677, A175
Wolfire, M. G., & Cassinelli, J. P. 1987, ApJ, 319, 850
Woodgate, B. E., Kimble, R. A., Bowers, C. W., et al. 1998, PASP, 110, 1183
Zinnecker, H. 2011, in ASP Conf. Ser. 440, UP2010: Have Observations Revealed a Variable Upper End of the Initial Mass Function?, ed. M. Treyer et al. (San Francisco, CA: ASP), 3